Int J Environ Res (2024) 18:75
https://doi.org/10.1007/s41742-024-00624-3

RESEARCH PAPER

Bentonite/Sesbania Gum Hydrogel for Effective Removal of Cationic Dyes: Network Structure Construction and the Role of Multiple Hydroxyl and Carboxyl Adsorption Sites

Luying Jiang[1] · Sishan Yu[1] · Jingwei Zhang[1] · Zisong Xu[2] · Rui Tang[3] · Yinlong Wang[3] · Ke Liang[4] · Chen Zhai[3] · Zhangfa Tong[3] · Hanbing Zhang[1]

Received: 6 December 2023 / Revised: 6 May 2024 / Accepted: 6 June 2024 / Published online: 23 June 2024

Abstract

Effective hydrogel adsorbents are widely used in toxic dyes removal, but weak toughness and inferior adsorption performance limit their actual application. Herein, a dual-functionalized epoxy and amino groups hyperbranched polysiloxane (HPSi) cross-linker was initially developed, bentonite (BT) was incorporated with sesbania gum (SG), acrylic acid/acrylamide (AA/AAm) was utilized as monomers to synthesize hydrogel adsorbent H-SG/BT(AA/AAm) for the adsorption of methylene blue (MB) and malachite green (MG). Various characterization techniques, adsorption parameters test and mechanism analysis demonstrated that HPSi and BT endowed H-SG/BT(AA/AAm) with enhanced mechanical strength (tentative extensibility of 2645% and elastic recovery was over 90%). The hydroxyl of BT and SG was completely insert into the hydrogel then significantly enhanced the swelling and adsorption capacity. H-SG/BT(AA/AAm) exposed a promising adsorption capacity towards MB and MG with maximum adsorption capacity of 1226 mg/g and 783 mg/g. Kinetic and isotherm studies indicated that the adsorption of MB and MG onto H-SG/BT (AA/AAm) closely followed the pseudo-second-order kinetic model and Langmuir isotherm. The adsorption efficiency of H-SG/BT (AA/AAm) for MB and MG could still reach 80% after five adsorption–desorption cycles. Clearly, H-SG/BT(AA/AAm) composites can be effectively utilized as an eco-friendly adsorbent for dyes adsorption in aqueous environments.

Highlights

- **H-SG/BT(AA/AAm) was successfully synthesized by hyperbranched polysiloxane (HPSi) crosslinker.**
- **HPSi and BT enhanced the mechanical properties of H-SG/BT(AA/AAm).**
- **SG and BT synergistically enhance the adsorption performance of H-SG/BT(AA/AAm).**
- **H-SG/BT(AA/AAm) exhibits high adsorption capacity for MB and MG.**
- **The adsorption mechanism of H-SG/BT(AA/AAm) was proposed.**

Keywords Bentonite · Sesbania gum · Mechanical properties · Adsorption mechanism · Cationic dyes

✉ Zhangfa Tong
zftong@gxu.edu.cn

[1] School of Resources, Environment and Materials, Guangxi University, Nanning 530004, China

[2] School of Civil Engineering and Architecture, Guangxi University, Nanning 530004, China

[3] Guangxi Key Laboratory of Petrochemical Resource Processing and Process Intensification Technology, School of Chemistry and Chemical Engineering, Guangxi University, Nanning 530004, China

[4] School of Mechanical Engineering, Guangxi University, Nanning 530004, China

Introduction

Synthetic dyes, with over 100,000 types and an annual production exceeding 700,000 tons, are prevalent in various industries (Saigl et al. 2023). Methylene blue and malachite green are among the toxic dyes, posing carcinogenic and teratogenic risks to life and damaging ecosystems (Khatooni et al. 2023; Vaid et al. 2023; Wang et al. 2021). Therefore, effective dye removal is crucial for water treatment, many effective strategy (like photocatalysis, electrochemical treatment, reverse osmosis, membrane separation and adsorption) have been used to remove toxic organic dyes (Hooshvar et al. 2024). Among them, the adsorption technology via hydrogels stands out for its simplicity and efficiency (Njuguna and Schönherr 2022). Hydrogels, with 3D polymer porosity structure, high water absorption, and active groups like –OH, –CONH–, and –COOH, provide a sustainable and efficient adsorption method for dye wastewater treatment (Wu et al. 2021; Zhu et al. 2023a, b; Khan et al. 2023). Reports have founded that advances in polymer science have yielded materials like magnetic molecularly imprinted polymers for targeted compound separation and sensitive sensors for detecting specific contaminants in water (Wang et al. 2023a, b, c; Shao et al. 2022). Furthermore, hydrogel materials exhibit a wide range of applications in water purification (Yan and Li 2021). Zhu et al. (2023a, b) created a graphene/polyacrylamide hydrogel with a 300% swelling capacity and 110.25 mg/g Ni^{2+} adsorption. Zhang et al. (2022) used laccase-immobilized hydrogels for 98.7% bisphenol A removal. Zhan et al. (2024) showcased hydrogels as sensors for automated irrigation control. Conductive PVA hydrogels, as in Xu et al. (2023), enhance flexible sensors in wearable tech and robotics. Bahaar et al. (2023) formulated PEG-based hydrogels for Sorafenib's controlled release, while Sidheekha et al. (2023) developed electroactive polyaniline/chitosan hydrogels for flexible supercapacitors.

Organic molecules containing a large number of functional groups, such as cellulose, chitosan, and gum, are extensively used as matrices for composite hydrogels. However, the available hydrogels suffer from issues such as susceptibility to cracking and breaking, low mechanical strength, and insufficient adsorption capabilities (Pandey et al. 2023; Yang et al. 2022). Studies suggest that the incorporation of polysaccharides into hydrogels has shown promise in improving their adsorption properties, environmental tolerance, and water retention abilities (Wu et al. 2021). Wei et al. (2016) introduced a natural hydrophilic polysaccharide into a PNIPAM hydrogel network via free radical polymerization, resulting in semi-interpenetrating network hydrogels that exhibited enhanced mechanical strength and excellent biocompatibility. Sesbania gum (SG) is a natural polysaccharide substance taken from the endosperm of sesbania japonica seed. The SG molecule consists of a β-1,4 glycosidic bond to mannose and its side chain has a single ring composed of α (1 → 6) glycosidic bond to galactose. Besides, the mannose and galactose are in a 2:1 ratio (Devkar et al. 2023). SG is decomposable, non-allergenic, and eco-conscious. The abundant ortho-cis hydroxyl groups in SG, along with its regular galactose side chain, can form hydrogen bonds with external organic and inorganic systems, potentially allowing for interactions with organic dyes. In addition, the molecular structure of SG contains the water-soluble part (63–68%) and the water-insoluble part. The water-soluble part gives SG higher water absorption and excellent swelling effect, which was favourable for adsorption of dyes, and the water-insoluble part makes SG have good stability in water. The crosslinking ability enables it to form highly elastic composite gel. Although studies on SG hydrogels have primarily focused on drug retardation and water retention agents. In our previous study, we found that SG could form stable SG-La beads with trivalent metal cations (La^{3+}, Fe^{3+}, etc.). The maximum adsorption capacity of AAB-SG-La beads incorporated with activated silica clay could reach 588 mg/g for Congo red (Yu et al. 2022). Whereas poor elasticity, recycling performance, poor structural integrity and easy dispersion limit sesbania gum hydrogel application. To address these issues, additional components like polymers, inorganic materials, and metals are often added to enhance its properties and expand its applications in adsorption-related fields (Ren et al. 2023).

Bentonite (BT), a common layered inorganic silicate mineral, is characterized by its interlayer cations that are exchangeable, facilitating exfoliation. This property, along with the abundance of hydrophilic moieties (–OH), allows BT to interact with organic polymers, creating heterogeneous materials that can bridge polymer chains via hydrogen linkage and homogenize the polymer network (Shirsath et al. 2011). Wang et al. (2023a, b, c) leveraged this interaction by introducing clay-based organic sheet silicates (COSS) into polyethylene (PE) and ethylene–vinyl acetate copolymer (EVA) blends. The COSS not only restricted the movement of molecular chains but also elevated the thermal decomposition temperature of the polymer matrix. Moreover, bentonite has better compatibility with polymers after organic modification and is uniformly dispersed in polymers. BT could provide more adsorption sites, both BT and SG have abundant –OH groups, the incorporation of bentonite into the SG hydrogel material enhances its adsorption capabilities through a synergistic effect (Jiang et al. 2022). Meanwhile, the crosslinking degree of the composite hydrogel was enhanced, resulting in a decrease in swelling ratio and the final adsorption capacity. Combining SG and BT can greatly enhance the mechanical

strength of the hydrogel and improve its thermal stability and chemical degradation resistance. Sekine et al. (2020) synthesized CMCF/CA/BT, which showed greater compressive strength (> 80 MPa) and better removal efficiency on MG and MB. Furthermore, owing to the loading effect of the hydrogel, the blend of bentonite in the hydrogel can also solve the problem of powder adsorbent materials unrecyclable and easily causing secondary pollution (Pandey 2017).

Toughening of hydrogels can also be achieved by developing novel crosslinkers into the hydrogel network. However, the commonly used cross-linking agent *N*,*N*-methylenebisacrylamide (MBAA) has limitations such as a short molecular chain, few reactive functional groups, and high toxicity. Hyperbranched polysiloxane are highly branched polymers that possess numerous functionalized groups (like amino and epoxy groups), which can provide sufficient adsorption active sites for dye molecules and enhance the mechanical properties of hydrogels (Chen et al. 2023). Li et al. (2019a, b) synthesized hyperbranched polysiloxane (HSi) with tunable molecular structures as a novel crosslinker to form the polyacrylamide/chitosan (PCH) hydrogels, confirmed that the tensile strength, elongation at break, and toughness of PCH1 hydrogels were higher than those of the PM hydrogels (crosslinker was MBAA). Considering the molecular structure and synthesis mechanism of commonly used hydrogel monomers (C=C double bond and free radical polymerization), the presence of functional groups enables HPSi to participate in the formation process of polymer networks as a crosslinker.

Therefore, we prepared a novel amine/epoxy dual-functional hyperbranched polysiloxane HPSi crosslinker to enhance the mechanical properties of hydrogels. Utilizing acrylamide (AAm) and acrylic acid (AA) as monomers, sesbania gum (SG) as a hydrogel matrix, incorporated with bentonite (BT) to synthesize H-SG/BT(AA/AAm) adsorbents for adsorbing MB and MG. SG and BT can significantly enhance the properties of hydrogels not only through the formation of hydrogen bonds and physical entanglements, but also by increasing the adsorption capacity via interactions between –OH groups and dyes. Moreover, HPSi strengthens polymer chain connections and hydrogel mechanics through monomer polymerization and macromolecule interactions. The effect of essential adsorption parameters (like monomer ratios, initial dye concentrations, adsorption time, pH, ionic strength, and temperature) and the swelling behavior of hydrogel were all examined. Additionally, the dye sorption process was characterized using adsorption isotherm, kinetic models, and thermodynamic analysis. Eventually, the adsorption mechanism and reuse performance of the hydrogel were further explored.

Materials and Methods

Materials

Acrylic acid (AA), acrylamide (AAm), sesbania gum (SG, $[C_6H_9O_5(CH_2COONa)]_n$, Fig. S1), (3-aminopropyl) triethoxysilane (KH550), and γ-glycidoxypropyl trimethoxysilane (KH560) were purchased from Macklin Chemical Regent Co., Ltd. (Shanghai, China). Potassium persulfate (KPS), sodium hydroxide (NaOH), hydrochloric acid (HCl), and sodium chloride (NaCl) were bought from Sinopharm Chemical Reagent Co., Ltd. (Beijing, China). Methylene blue (MB) and Malachite green (MG) were obtained from Macklin Chemical Regent Co., Ltd. (Shanghai, China). Bentonite (BT) was provided by Guanghua Regent Co., Ltd. (Guangdong, China). All reagents used in the experiments were analytical grade and ultrapure water was used in whole experiments.

Fabrication of H-SG/BT(AA/AAm) Adsorbent

The adsorbent H-SG/BT(AA/AAm) was synthesized using the free radical copolymerization method. Sesbania gum solution was prepared in hot (60 °C) ultrapure water at a concentration of 2 wt%. Then, 2 g bentonite (BT) was dissolved in 30 mL 2 wt% SG solution with magnetic stirring for 3 h. Subsequently, 6 g AAm, 15.6 mL AA solution neutralized with NaOH, and 0.6 g HPSi were added into the SG/BT suspension successively and stirred thoroughly. After, 0.1 g of KPS was added to the general mixture as an initiator and stirred for 10 min. Eventually, the mixture was through a vacuum oven drying at 80 °C for 3 h to obtain H-SG/BT(AA/AAm). Furthermore, the synthesis of H-SG/BT(AAm), H-SG(AA/AAm), and H-BT(AA/AAm) has been done according to the mentioned method (Scheme 1).

Swelling determination of H-SG/BT(AA/AAm)

A higher swelling ratio increases the pores between macromolecular chains in hydrogels and exposes active sites to water and dye molecules that make adsorption equilibrium reach rapidly (Yan and Li 2021; Mokhtar et al. 2020). The swelling behaviors of H-SG/BT(AA/AAm) were investigated using gravimetric analysis. Firstly, the vacuum freeze-dried hydrogel samples (W_0) and subsequently immersed in deionized water (DW) with a volume of 100 mL. The samples were taken out from DW at a predetermined time and gently blotting the surface moisture with filter paper. Finally, the swollen hydrogel samples proceeded to weigh (W_t). The effects of swelling time, pH, and salt solution on the swelling properties of composite hydrogel were determined. All experiments within the

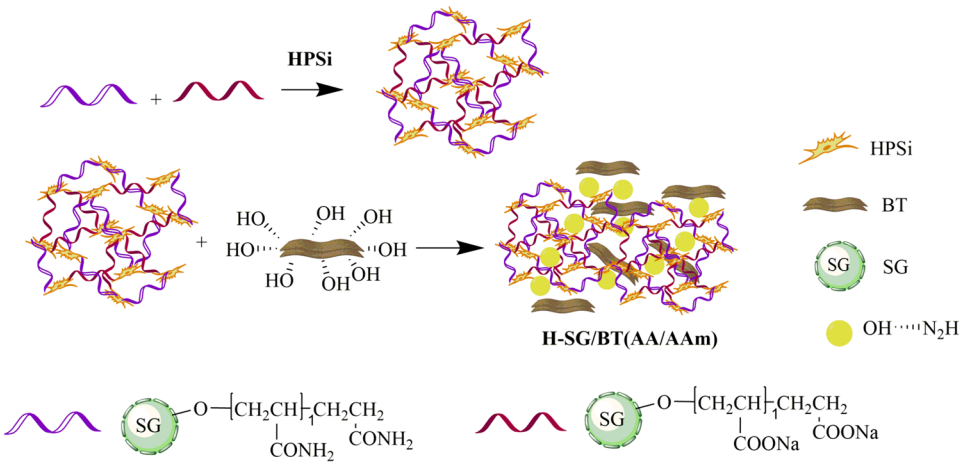

Scheme 1 Schematic illustration of the synthetic mechanism of H-SG/BT(AA/AAm)

study were repeated three times. The swelling ratio (SR) of hydrogel adsorbents was employed using the Eq. (1)

$$\mathrm{SR} = \frac{W_t - W_0}{W_0} \tag{1}$$

where W_0 (g) and W_t (g) are the weight of the dry and swollen hydrogel samples, respectively. To get an accurate value, four hydrogel samples were tested and used the mean to evaluate the swelling behavior of the hydrogel.

Characterization

Fourier transform infrared spectrophotometer (FT-IR) analysis of H-SG/BT(AA/AAm) adsorbent was performed with a Shimadzu IRTracer-100 FTIR spectrometer (400–4000 cm^{-1}). The hydrogel morphology was examined using a field emission scanning electron microscope (FE-SEM, SU8220 S-3400 N, Hitachi, Japan). The pore size and specific surface area of H-SG/BT(AA/AAm) were obtained using the Brunauer–Emmett–Teller (BET) method. Energy dispersive X-ray spectroscopy (EDS) was employed to determine the elemental distribution on the surface of composite hydrogels. XRD analysis was completed on BT, SG, H-SG/BT(AAm), H-SG(AA/AAm), and H-SG/BT(AA/AAm) using a D/max 2500 V X-Ray diffractometer (Rigaku, Japan) with Cu kα radiation (λ = 1.5406 Å) at a scan rate of 10°/min in the 5°–80° (2θ). The H-SG/BT(AAm), H-SG(AA/AAm) and H-SG/BT(AA/AAm) were also analyzed on a TAQ500 thermogravimetric analyzer under a nitrogen atmosphere with a rate of 10℃/min in the temperature range of 25–800 °C. A Shimadzu UV–Vis spectrophotometer was used to investigate the adsorption behavior of MB and MG on the hydrogel (UV-2550, Shimadzu, Japan).

The zero-charge point (pH_{pzc}) of composite hydrogels was determined using the pH drift equilibrium technique. Four conical flasks with 100 mL of 0.01 M NaCl were used as electrolytes, and pH was varied from 2 to 10 using 0.1 M HCl and NaOH. 0.1 g composite hydrogel was added to each flask and oscillated for 48 h. The final pH measured after 48 h was plotted versus the initial pH and the intersection point was taken as pHzpc of the composite hydrogels.

A WDW-05L tensile machine with a 100 mm/min stretching speed was used to assess the tensile strength at room temperature. The hydrogel samples were divided into 5 mm thick dumbbell shapes (10 mm in length and 5 mm in width). The tenacity of hydrogel samples was determined by calculating the integral of stress–strain relationship during tensile testing. The cylindrical hydrogel (20 mm in diameter and 20 mm in height) was subjected to compression testing at a rate of 100 mm/min, within a maximum compressive deformation of 90%.

Adsorption Studies of H-SG/BT(AA/AAm)

The adsorption of MB and MG cationic dyes was done in the batch system using H-SG/BT(AA/AAm). The adsorption study was performed in pH 2–10, 100 mL MB and MG solution with concentration of 20–800 mg/L, adsorbent dose of 0.5 g/L, contact time of 0–48 h, temperature of 25–65 °C and salinity of 0–1 wt%. The effect of AA/AAm monomer ratios and effective parameters like pH, temperature, contact time, salinity, and dye concentrations on the adsorption behaviors was investigated. The residual dye in an aqueous solution was measured using a UV–Vis spectrophotometer at a maximum wavelength of 664 nm and 617 nm. The adsorption process underwent three iterations and the average of the data was presented as the desired result.

The equilibrium adsorption capacity (q_e) and percent removal ratio (R%) involved considering dye solution concentrations in which H-SG/BT(AA/AAm) was added before (C_0) and after adsorption (C_e). For this, Eqs. (2) and (3) below were used.

$$q_e = \frac{(C_0 - C_e) \times V}{m} \quad (2)$$

$$\mathrm{R} = \frac{C_0 - C_e}{C_0} \times 100\% \quad (3)$$

where q_e (mg/g) is the amount of dye absorbed when the reaction reached equilibrium. C_0 and Ce (mg/L) are the initial and equilibrium concentration of dye solutions, m (mg) is the amount of hydrogel used and V (L) is the MB/MG solution volume.

Reusability Studies

Reusability is a critical parameter for evaluating the adsorption performance of an adsorbent in actual applications. Therefore, adsorption–desorption experiments were carried out five cycles to investigate the reusability of H-SG/BT(AA/AAm). The experimental procedure involved desorbing the saturated hydrogel samples, which had adsorbed MB and MG, using 0.1 mol/L HCl for a duration of 4 h. Afterward, the desorbed hydrogel was washed and neutralized with deionized water several times to prevent any potential impact of HCl on H-SG/BT(AA/AAm). The collected desorbed hydrogel was dried at 65 °C to prepare it for the subsequent adsorption cycle, allowing for a comparison of the impact of different cycles on the adsorption capacity.

Results and Discussion

Characterization of H-SG/BT(AA/AAm)

Functional Group Analysis of Composite Hydrogels

To analyze the structure characterization and chemical bonds of the composite hydrogel, FT-IR spectroscopy is employed. The resulting FT-IR spectra for samples AA, AAm, SG, BT, and H-SG/BT(AA/AAm) are presented in Fig. 1a. AAm displayed the asymmetric and symmetric stretching vibration peaks of N–H in amide bond at 3369 cm^{-1} and 3196 cm^{-1}, respectively. 1673 cm^{-1} and 1611 cm^{-1} was the stretching vibration peaks of C=O group in amide-I (Jiang et al. 2023). The peaks at 1659 cm^{-1}, 1551 cm^{-1}, and 1458 cm^{-1} showed the stretching vibrations of –COONa in the AA structure, while 1405 cm^{-1} was attributed to the –COOH flexural vibration. The characteristic absorption bands observed at 1039 cm^{-1} correspond to the Si–O–Si stretching vibration in BT structure (Mamytbekov et al. 2023). The absorption peaks at 3454 cm^{-1} and 2954 cm^{-1} related to the stretching vibrations of O–H and C–H groups were observed in SG (Flores-Cespedes et al. 2023). The 917 cm^{-1} characteristic peak related to epoxy groups matches the 920 cm^{-1} epoxy group characteristic peak of HPSi in H-SG/BT(AA/AAm), indicating that the presence of covalent bonds between the epoxy and hydroxyl groups in SG molecule. Focusing on magnified FT-IR spectra ranging from 1400 to 1800 cm^{-1}, characterized peaks attributed to amide I (C=O stretching), amide II (N–H flexural vibration) and the carbonyl bending vibration of –COOH were presented at 1670 cm^{-1}, 1622 cm^{-1}, and 1408 cm^{-1}, respectively. Additionally, the peaks at 1658 cm^{-1}, 1560 cm^{-1}, and 1456 cm^{-1} related to –COONa carbonyl stretching vibration (Devkar et al. 2023). The H-SG/BT(AA/AAm) maintained the absorption peaks of AA and AAm, with shifted positions due to their polymerization. Moreover, the presence of BT broadened the O–H stretching vibration at 3462 cm^{-1}, which is likely due to hydrogen bond occurrence in the polymer and BT (Lan et al. 2019). These observations confirmed that H-SG/BT(AA/AAm) has been successfully synthesized with abundant chemical moieties (–COOH, $–NH_2$, and –OH), which are beneficial for eliminating dyes from wastewater.

Crystal Structure Analysis of Composite Hydrogels

XRD analysis is one of the most effective methods to investigate the crystalline solids phase of hydrogel materials. The XRD patterns of BT, SG, H-SG/BT(AAm), H-SG(AA/AAm), and H-SG/BT(AA/AAm) are illustrated in Fig. 1b. A distinct diffraction peak at $2\theta = 20.13°$ was observed in SG, which is caused by the semi-crystalline nature of SG (Tang et al. 2020). The diffraction peak of H-SG(AA/AAm) at $2\theta = 20.13°$ became wider and its intensity diminished. Grafting of AAm and AA caused a decrease in the overall crystallinity of H-SG(AA/AAm) (Abdel-Bary and Elbedwehy 2018). The peaks at 2θ of 5.72°, 19.70°, 26.64° and 61.99° in the BT spectrum were indicative of montmorillonite (Santoso et al. 2023). In addition, the reflection peaks at $2\theta = 21.84°$ corresponded to quartz in the BT sample, indicating the main components of BT are montmorillonite and SiO_2 (Khan et al. 2020). Both H-SG(AA/AAm) and H-SG/BT(AA/AAm) showed characteristic diffraction peaks of montmorillonite and quartz at 2θ of 19.70° and 26.64°, but with weaker intensity, suggesting that BT is fully dispersed and exfoliated within the hydrogels (Ghafelebashi et al. 2018). A decrease in the diffraction peak of hydrogels was observed in the spectrum, indicating the associations among AA, AAm, SG, and BT involve hydrogen bonding, as supported by the FTIR analysis results (Dai et al. 2018).

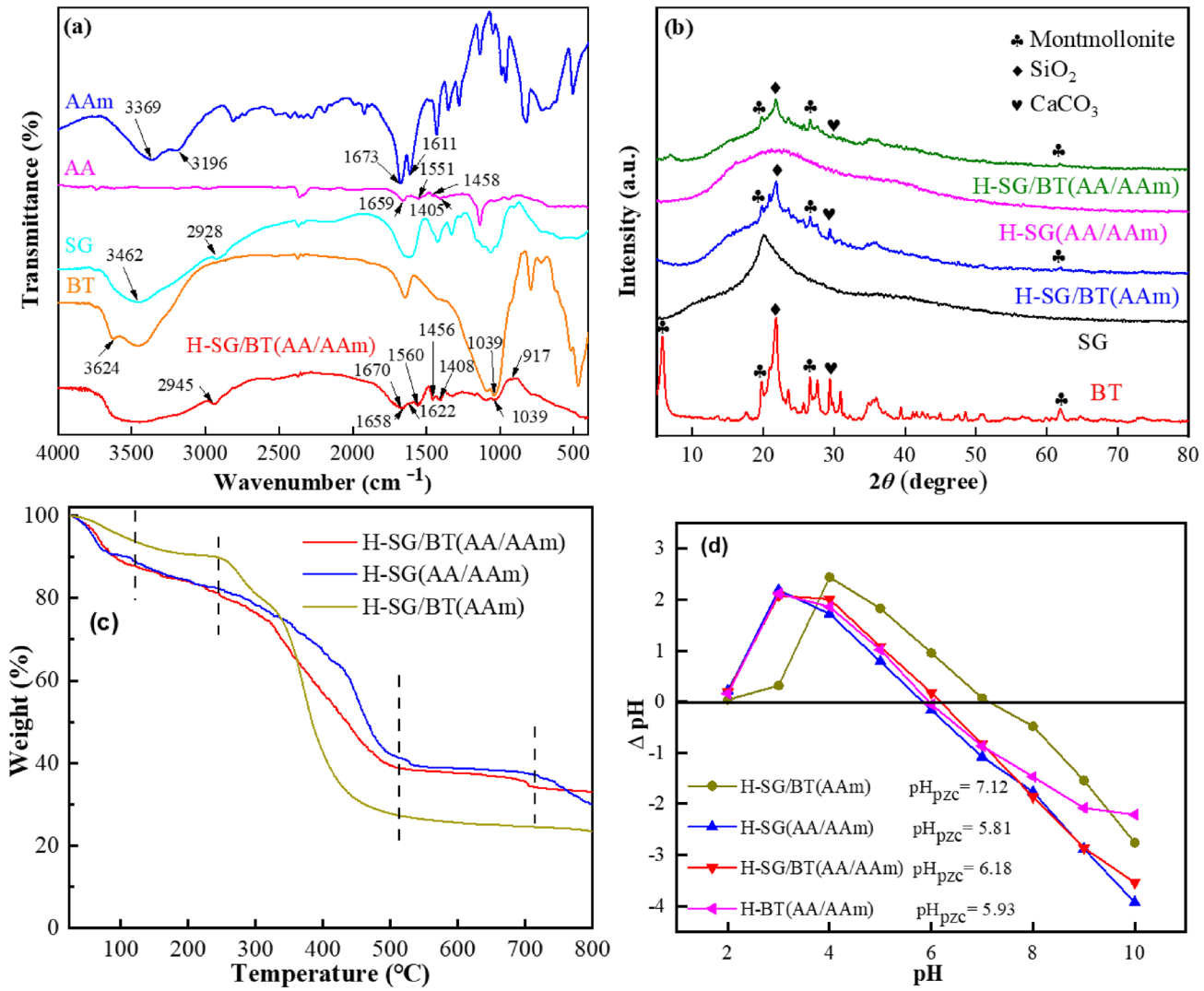

Fig. 1 **a** FTIR spectra of AA, AAm, BT, SG, H-SG/BT(AA/AAm); **b** XRD spectra of SG, BT, H-SG/BT(AAm), H-SG(AA/AAm) and H-SG/BT(AA/AAm); **c** TGA spectra of H-SG/BT(AAm), H-SG(AA/AAm) and H-SG/BT(AA/AAm); **d** pH_{pzc} of H-SG/BT(AAm), H-SG(AA/AAm), H-BT(AA/AAm) and H-SG/BT(AA/AAm)

Thermal Stability Analysis of Composite Hydrogels

Thermogravimetric analysis (TGA) is a method used to determine the thermal stability and composition of materials as a function of increasing temperature. The TGA results of H-SG/BT(AAm), H-SG(AA/AAm), and H-SG/BT(AA/AAm) samples are depicted in Fig. 1c. Based on the desired figure, the samples in the temperature of 25–800 °C have four steps of weight loss. The initial step involved a 12% weight loss for composite hydrogels occuring at 25–121 °C, which is attributed to water evaporation (Ghadami et al. 2022). The second weight loss occurred at 121–243 °C, resulting in a 7% weight loss due to the degradation of composite hydrogel components into CO_2 at elevated temperatures. In the temperature range of 243–511 °C, the hydrogel undergo a 42% weight loss because of the C–O–C groups and AA/AAm polymer chains decomposition within hydrogel skeleton. In the final stage, the hydrogel lost 4% weight when the temperature increased from 511 to 707 °C, which was relevant to the minimal non-volatile residue in the hydrogel. TGA analysis demonstrates that the H-SG/BT(AA/AAm) has greater thermal stability than H-SG/BT(AAm), with the overall weight loss decreasing from 77 to 67%. In the third stage, the H-SG/BT(AA/AAm) hydrogel weight loss peak moved from 430 °C to a higher temperature of 511 °C, which is ascribed to the –COOH (from AA) acting as an anchor between the polymer chains and the bentonite (Melendez-Ortiz et al. 2022; Wang et al. 2019). The inclusion of AA polymer in H-SG/BT(AA/AAm) imparts a more rigid structure and confers higher

thermostability of the hydrogel. Compared to H-SG(AA/AAm), H-SG/BT(AA/AAm) had less weight loss as the cross-linked mesh structure formed by interweaving of SG and AA/AAm with the BT lamellar structure likely enhances the cross-linking architecture (Wang et al. 2022; Pereira et al. 2020). These findings clearly demonstrate that the integration of BT bolsters the thermostability and strength of H-SG(AA/AAm).

Zeta Potential Analysis of Composite Hydrogels

The surface charge of the adsorbents in an aqueous solution is characterized by the point of zero charge. The pH_{pzc} of the composite hydrogels were determined using zeta potential analysis. As presented in Fig. 1d, the adsorbent surface becomes negatively charged when $pH > pH_{pzc}$, thereby favoring the adsorption of cationic dyes (MB^+ and MG^+) due to the electrostatic force. The pH_{pzc} of H-SG/BT(AAm), H-SG(AA/AAm), H-BT(AA/AAm), and H-SG/BT(AA/AAm) were found to be 7.12, 5.81, 5.93, and 6.18 respectively. In acidic conditions, the –COOH and –OH groups are protonated, exhibiting electrostatic competition between the positively charged adsorbent and the cationic dye molecules (Khatooni et al. 2023). Additionally, reducing the concentration of H^+ can increase the available negatively charged sites and surface area for cationic dyes to be located in hydrogel. Consequently, this improves adsorption efficiency of hydrogel adsorbents through electrostatic forces (Myint et al. 2020; Benhouria et al. 2015).

Morphological Structure Analysis of Composite Hydrogels

The morphological structures of freeze-dried H-SG/BT(AAm), H-SG(AA/AAm), H-BT(AA/AAm), and H-SG/BT(AA/AAm) as observed in Fig. 2. The network structure of H-SG/BT(AAm) was highly dense with the smallest pore size (Fig. 2a), suggesting a high degree of crosslinking between the monomer AAm and the matrix SG. Furthermore, the BT within H-SG/BT(AAm) is not unevenly encapsulated, which may be due to the alkyl chains of SG reducing the interaction of hydrophilic groups (Wang and Wang 2010), thereby enhancing the compatibility between the polymer and BT. Although H-SG/BT(AAm) possesses good mechanical properties, its swelling degree is also compromised due to the dense network structure. The H-SG(AA/AAm) exhibited a thicker wrinkled structure with larger pores (Fig. 2b), which may reduce the adsorptive specific surface area and the compressive elastic recovery performance to some extent. This effect could be detrimental to both the adsorption capacity and the recyclability of H-SG(AA/AAm). In comparison, H-BT(AA/AAm) featured smaller surface wrinkles, fewer pores, and smaller pore sizes (Fig. 2c). Moreover, the encapsulation of BT particles by the polymer was uneven, likely due to the lower degree of polymerization between the AA and AAm monomers. This reduced compatibility with BT in the absence of SG, consequently diminishing the adsorption capacity and tensile performance of H-BT(AA/AAm). In contrast, H-SG/BT(AA/AAm) featured a three-dimensional network

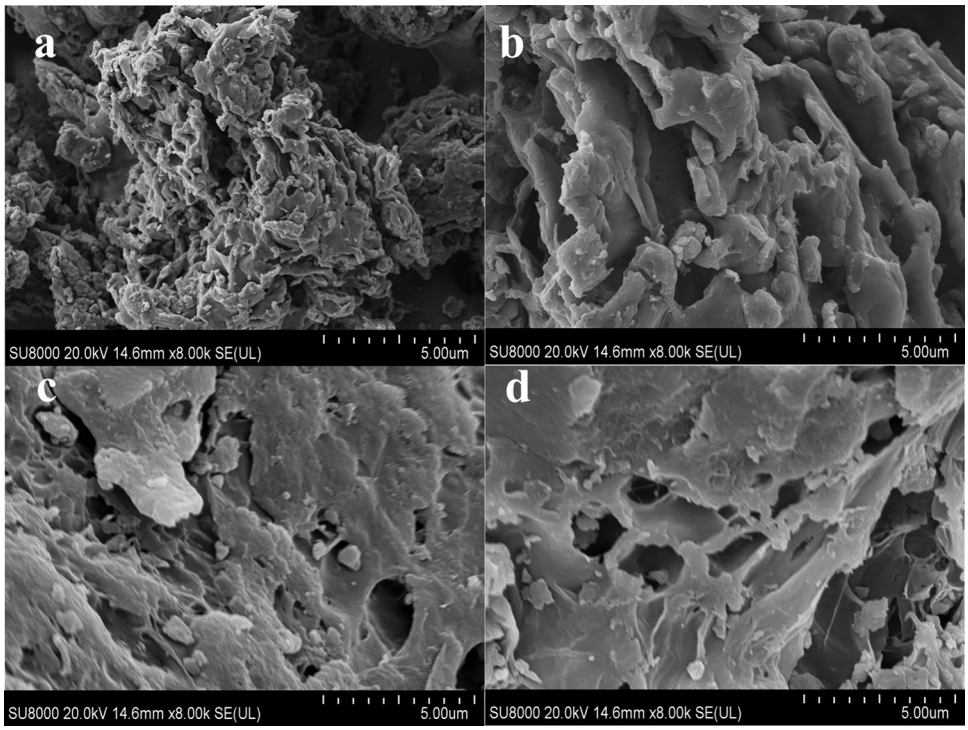

Fig. 2 SEM images of H-SG/BT(AAm) (**a**), H-SG(AA/AAm) (**b**), H-BT(AA/AAm) (**c**), and H-SG/BT(AA/AAm) (**d**)

structure with numerous fine wrinkles and smaller pore sizes (Fig. 2d), which was more conducive to optimal adsorption performance and also endowed the material with suitable mechanical properties, ensuring its recyclability. In summary, the introduction of SG not only promotes the uniform dispersion of BT within H-SG/BT(AA/AAm) but also provides a network structure for H-SG/BT(AA/AAm) through moderate crosslinking with AA/AAm. Moreover, the BET analysis results are summarized in Table S3. BET surface area for H-SG/BT(AA/AAm) was 0.0783 m^2/g, indicating the porous structure made H-SG/BT(AA/AAm) efficiently capture molecule of dyes (Shi et al. 2023).

Swelling Properties of Composite Hydrogels

Testing the swelling ratio is crucial for optimizing the hydrogel's performance in absorbing contaminants, as a higher swelling capacity typically translates to a larger surface area for interaction with pollutants. Therefore, the swelling behavior of the hydrogels was investigated. The swelling curves of H-SG/BT(AAm), H-SG(AA/AAm), H-BT(AA/AAm), and H-SG/BT(AA/AAm) are depicted in Fig. S4. The swelling trends of all hydrogels were similar: they initially swollen rapidly, followed by a slow and equilibrium state. The water absorption process of H-SG/BT(AA/AAm) can be characterized by two distinct stages: initially, the carboxyl groups of H-SG/BT(AA/AAm) establish hydrogen bonding interactions with water molecules, resulting in the adsorption of water and subsequent hydrogel swelling. As the hydrogel absorbs water and undergoes swelling, its network structure expands. This expansion initiates hydrolysis of its hydrophilic groups, generating ions and establishing a concentration gradient with the surrounding aqueous solution. The internal network structure of the hydrogel is continuously infiltrated by water molecules until the osmotic pressure inside and outside becomes balanced, which maximizes its swelling capacity and achieves swelling equilibrium (Ozsoy et al. 2022). The swelling ratio of H-SG/BT(AAm), H-SG(AA/AAm), H-BT(AA/AAm), and H-SG/BT(AA/AAm) were 77 g/g, 505 g/g, 358 g/g, and 501 g/g, respectively. The incorporation of SG into H-BT(AA/AAm) resulting in the hydrogel's swelling ratio increase from 358 to 501 g/g, which was attributed to the hydrophilic groups (–OH) present in SG have a strong propensity to form hydrogen bonds with water molecules. Compared to H-SG(AA/AAm), the incorporation of BT into H-SG(AA/AAm) increased crosslinking network density, resulting in the hydrogel's swelling ratio decrease from 505 to 501 g/g. The hydrogel exhibited a deswelling state at 24–48 h, because of the hydrogen bonding between protonated carboxyl groups and amide groups along the hydrogel molecular chains then brought release of excess moisture. It was evident that the amount of released water from H-SG/BT(AA/AAm) was less than that from H-SG(AA/AAm), because the BT inclusion enhanced water retention (Elsaeed et al. 2022). A higher cross-linking degree corresponds to a low swelling capacity (Chang et al. 2022). The cross-linking degree of H-SG/BT(AAm) is higher than that of H-SG/BT(AA/AAm). Additionally, carboxyl groups have a higher affinity for forming hydrogen bonds with water than amide groups. Consequently, H-SG/BT(AAm) showed a reduced ability to swell in comparison to H-SG/BT(AA/AAm), which was also consistent with the mechanical property changes observed in the hydrogels.

The pH significantly influences the ionization process and the availability of adsorption sites, therefore the impact of solution pH on the swelling behavior of the hydrogels was investigated across a pH range from 2 to 10. As illustrated in Fig. 3a, the swelling ratios of H-SG/BT(AAm), H-SG(AA/AAm), H-BT(AA/AAm), and H-SG/BT(AA/AAm) were 12 g/g, 3 g/g, 3 g/g and 4 g/g at pH 2. The presence of a large amount of H^+ in the extreme acid condition inhibited the ionization of carboxyl and amide groups. The formation of intramolecular hydrogen bonds between an excessive amount of H + ions and these groups caused the hydrogels to contract. As the pH value increased, the –COOH

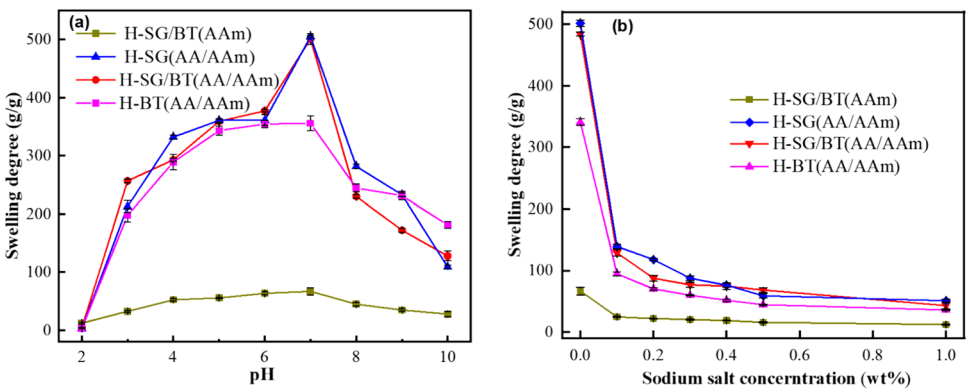

Fig. 3 The swelling curves of H-SG/BT(AAm), H-SG(AA/AAm), H-BT(AA/AAm), and H-SG/BT(AA/AAm) hydrogels in **a** different pH solutions and **b** varied salt solutions

and $–NH_2$ groups became ionized, which enhanced electrostatic repulsion and subsequently increased hydrogel swelling. The maximum swelling values of H-SG/BT(AAm), H-SG(AA/AAm), H-BT(AA/AAm), and H-SG/BT(AA/AAm) at pH 7 corresponded to 67 g/g, 356 g/g, 505 g/g and 501 g/g, respectively. It was noticed that the swelling ratios of four hydrogels decreased when the pH exceeded 7. This is because the OH^- in the solution can neutralize with the acrylic acid of the hydrogels, resulting in the generation of sodium acrylate on the polymeric molecular chains (Li et al. 2023). Furthermore, due to the Na^+ ionization of the sodium acrylate, the permeability between the inside and outside of the hydrogels decreased with the increase of Na^+ within the solution. This phenomenon hinders the movement of water molecules into hydrogels, leading to a decrease in swelling ratios (Ghumman et al. 2022).

To investigate the salinity tolerance of hydrogels, we immersed them in different concentrations of sodium chloride solutions (0.1–1 wt%) for 24 h. The ionic strength of salt solutions on swelling of hydrogels is illustrated in Fig. 3b. As the Na^+ concentration increased from 0 to 1 wt%, the swelling ratios of H-SG/BT(AAm), H-SG (AA/AAm), H-BT(AA/AAm), and H-SG/BT(AA/AAm) correspondingly decreased from 67 g/g, 502 g/g, 341 g/g and 484 g/g to 12 g/g, 51 g/g, 36 g/g and 43 g/g, respectively. It was observed that the swelling ratios of hydrogels diminished with the concentration of salt solutions increased. This drastic decrease in the swelling ratio is attributed to the reverse osmosis process. The increased ionic strength of swelling media then reduced osmotic pressure between external medium and internal polymer network. Because of the inhibition of $–COO^-$ dissociation by Donnan equilibrium, a decrease of osmotic pressure and swelling capacity of hydrogels occurred (Matsuda et al. 2019). Additionally, the shielding effect of Na^+ and cations encircled the carboxylate ions led to a reduction of electrostatic repulsion, which in turn caused swelling ratios to decrease. Sodium salts can inhibit the effect of polymer chain relaxation, and a high concentration of Na^+ caused self-polymerization of polymer chains in hydrogels then decreased swelling ratios (Bashir et al. 2018).

Mechanical Property Analysis of Composite Hydrogels

Assessing the mechanical properties of hydrogels is crucial for ensuring their durability over an extended period. Figure 4 illustrates the photographs of H-SG/BT(AA/AAM) (w = 5.0 mm, h = 2.0 mm) hydrogel in different mechanical conditions. Figure 4 illustrates the photographs of H-SG/BT(AA/AAM) (w = 5.0 mm, h = 2.0 mm) hydrogel in different mechanical conditions. As shown in Fig. 4a, H-SG/BT(AA/AAm) was able to lift a bottle with a load-bearing of 500 g full water. The absence of cracks and fractures indicates that the H-SG/BT(AA/AAm) possesses excellent mechanical traits. The H-SG/BT(AA/AAm) displayed exceptional elasticity, with up to 400% elongation and could be knotted without any mechanical damage (Fig. 4b, c).

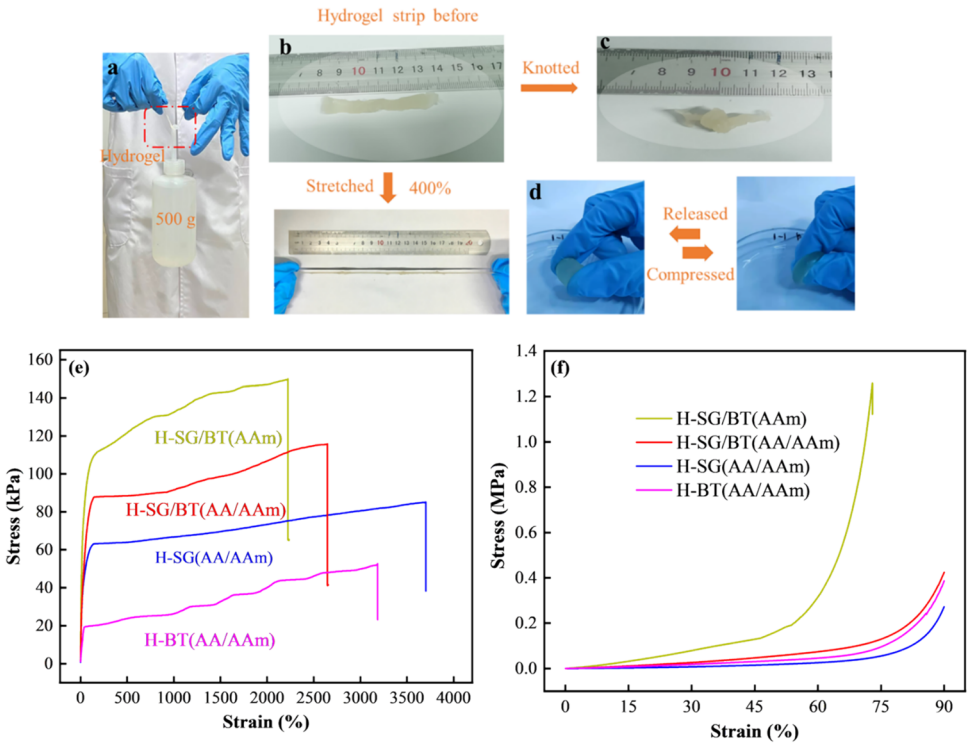

Fig. 4 Photographs of the H-SG/BT(AA/AAm) after sustaining a weight of 500 g (**a**), stretching (**b**), knotting (**c**), and compression (**d**); tensile properties of various composite hydrogels (**e**); compressive properties of various composite hydrogels (**f**)

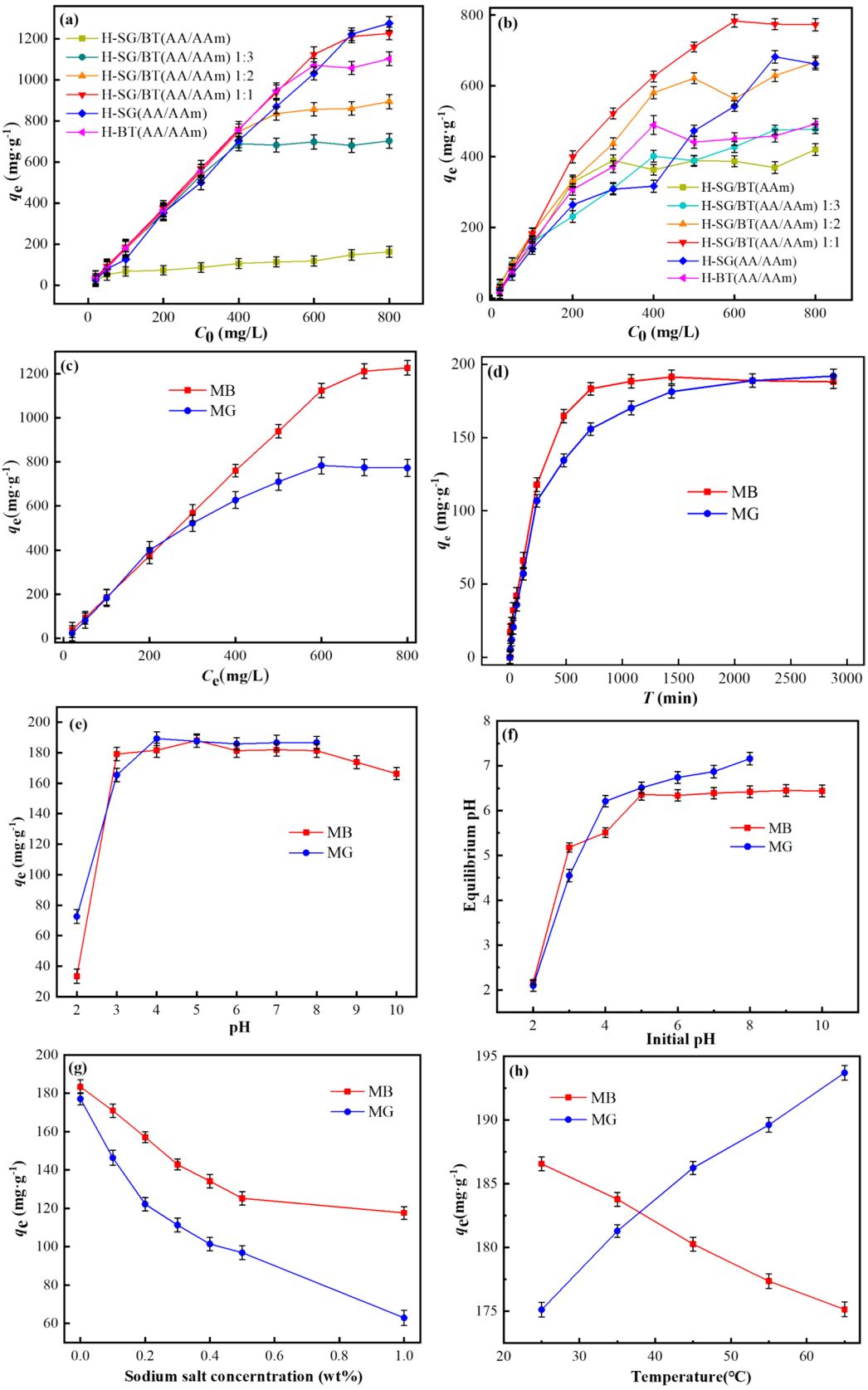
(a)
H-SG/BT(AA/AAm)
H-SG/BT(AA/AAm) 1:3
H-SG/BT(AA/AAm) 1:2
H-SG/BT(AA/AAm) 1:1
H-SG(AA/AAm)
H-BT(AA/AAm)
q_e (mg·g^{-1})
C_0 (mg/L)
(b)
H-SG/BT(AAm)
H-SG/BT(AA/AAm) 1:3
H-SG/BT(AA/AAm) 1:2
H-SG/BT(AA/AAm) 1:1
H-SG(AA/AAm)
H-BT(AA/AAm)
q_e (mg·g^{-1})
C_0 (mg/L)
(c)
MB
MG
q_e(mg·g^{-1})
C_e(mg/L)
(d)
MB
MG
q_e (mg·g^{-1})
T (min)
(e)
MB
MG
q_e (mg·g^{-1})
pH
(f)
MB
MG
Equilibrium pH
Initial pH
(g)
MB
MG
q_e (mg·g^{-1})
Sodium salt concerntration (wt%)
(h)
MB
MG
q_e(mg·g^{-1})
Temperature(°C)

◂**Fig. 5** The effect of different monomer ratios (**a**, **b**), dyes initial concentration (**c**), contact time (**d**), initial pH (**e**), salt concentrations (**g**), and temperature (**h**) on the adsorption capacity of MB and MG by H-SG/BT(AA/AAm); **f** equilibrium pH of MB and MG adsorption by H-SG/BT(AA/AAm)

After undergoing high-intensity squeezing deformation, the composite hydrogel (d × h: 20.0 mm × 20.0 mm) promptly returned to its initial shape, showcasing its remarkable toughness (Fig. 4d).

Figure 4e shows the tensile characteristics of various composite hydrogels. The H-SG/BT(AA/AAm) demonstrated a tension strength of 116 kPa, a snap elongation of 2645%, and a fracture work of 257 kJ/m^3. These mechanical properties were significantly superior to those of the H-SG/BT(AA/AAm)-M cross-linked with conventional agents (42 kPa, 326%, and 11 kJ/m^3), respectively. The fracture work of H-BT(AA/AAm) reached 112 kJ/m^3, lower than that of H-SG/BT(AA/AAm), suggesting that SG enhances the toughness of the composite hydrogel. As shown in Fig. 4f, the compression strength of H-SG/BT(AA/AAm) was 0.43 MPa, significantly better than MBAA hydrogel (0.10 MPa). It also slightly surpassed the H-SG(AA/AAm) (0.27 MPa) and H-BT(AA/AAm) (0.39 MPa), signaling that the combination of BT and SG enhances the mechanical performance. The interaction between reactive groups (–COOH, $–NH_2$, and –OH) of polymer chains and BT (–OH) generates additional cross-linking sites. Adjusting the AA to AAm ratio modifies the mechanical strength and deformation of the hydrogel. Short-chain breaks absorb mechanical energy and increase tensile strength, while long-chain polymers maintain elasticity. The mechanical properties are attributed to several enhancement mechanisms, including polymer chain fracture, cross-linking of multifunctional groups, and compounding of components at various scales (Du et al. 2016).

Analysis of Adsorption Behavior

Effect of Monomer Ratios on MB and MG Adsorption

Exploring the impact of monomer ratios in the synthesis of hydrogels on the adsorption of MB and MG is crucial for tailoring the adsorbent properties to achieve optimal dye removal efficiency. Therefore, the adsorption effects of H-SG/BT(AA/AAm) with different monomer ratios (m(AA/AAm) = 1:3, 1:2, 1:1), H-SG/BT(AAm), H-SG(AA/AAm), and H-BT(AA/AAm) on MB and MG were investigated. As presented in Fig. 5a, b, the H-SG/BT(AAm) exhibited a maximum adsorption capacity of 162 mg/g for MB and 420 mg/g for MG. Subsequently, the adsorption capacities of H-SG/BT(AA/AAm) for MB (increased from 703, 895 to 1226 mg/g) and MG (increased from 478, 668 to 783 mg/g) were further enhanced with a higher acrylic acid content (m(AA/AAm) ratio ranging from 1:3 to 1:1). These interactions are attributed to –COOH/–OH groups of the hydrogel interacting with MB and MG molecules, and the carboxyl groups exhibited a stronger adsorption affinity for MB and MG than the amide groups. The adsorption capacity of MB (1103–1226 mg/g) and MG (662–783 mg/g) has increased after adding SG to H-BT(AA/AAm). It was attributed to the electrostatic attraction between the SG and dye molecules, facilitating dye adsorption onto the hydrogel. A decrease in MB adsorption capacity from 1275 to 1226 mg/g and an increase in MG adsorption capacity from 492 to 783 mg/g after adding BT into H-SG(AA/AAm). This could be attributed to the BT enhanced cross-linking degree of the hydrogel then reducing the available active sites for MB adsorption. Considering the influence of AA on the adsorption and mechanical properties, the H-SG/BT(AA/AAm) with a molar ratio of AA to AAm of 1:1 was selected as the adsorbent to subsequently investigate the adsorption properties of MB and MG.

Effect of Initial Dye Concentrations and Contact Time on Adsorption

The effect of initial MB and MG concentration (range from 20 to 800 mg/L) on the adsorption capacity of H-SG/BT(AA/AAm) was investigated with 0.5 g/L adsorbent dosage. The MB and MG solutions were shaken in a water bath shaker at 25 °C for 720 and 1080 min, respectively. The resulting adsorption capacity of H-SG/BT(AA/AAm) with various initial concentrations of MB and MG are shown in Fig. 5c. With increasing initial concentrations of MB and MG, the adsorption efficiency of MB and MG initially showed an increasing trend then followed by a plateau. This was because the occupation of more saturated reaction sites on the H-SG/BT(AA/AAm) for dye molecules to locate. Besides, higher interaction of dye molecules with the surface and active sites in the adsorbent structure could be the cause for the high removal efficiency at low MB and MG concentrations. As dye concentration increased, due to the adsorbent sites of H-SG/BT(AA/AAm) became saturated, and competition between dye molecules for the limited active sites of H-SG/BT(AA/AAm). Consequently, the dye adsorption capacity decreased with higher initial dye concentrations. H-SG/BT(AA/AAm) exhibited maximum adsorption capacities of 1226 mg/g for MB at a concentration of 800 mg/L, and 783 mg/g for MG at a concentration of 600 mg/L.

Establishing equilibrium in dye adsorption is contingent upon a critical factor: the contact time. The effect of contact time on MB and MG adsorption by H-SG/BT(AA/AAm) was studied with 100 mg/L of MB and MG, contact time of 0–48 h. Figure 5d shows the adsorption capacity

increased rapidly in the initial 8 h, which was attributed to the presence of abundant active sites on the hydrogel surface. As the contact time increased from 5 to 720 min, the adsorption capacity of H-SG/BT(AA/AAm) for MB raised from 17 to 183 mg/g, while for MG escalated from 5 to 156 mg/g. The adsorption capacity of H-SG/BT(AA/AAm) for dyes raised slowly until it reached adsorption equilibrium at 1440 min. There was a positive correlation between the adsorption capacity and efficiency of the hydrogel with increasing adsorption time, as the adsorption sites remained unsaturated at initial period. Specifically, H-SG/BT(AA/AAm) achieved removal efficiency of 92% for MB after 720 min and 85% for MG after 1080 min. The dye removal capacity stabilized as the polymer's active sites reached saturation, maintaining a constant quantity post-optimization. Considring the adsorption efficiency and capacity, the optimal adsorption times of H-SG/BT(AA/AAm) for MB and MG were 720 and 1080 min, respectively.

Effect of pH on MB and MG Adsorption

Solution pH is one of the most critical factors that manipulate the adsorption behavior since it affects both dye molecules and the surfaces of hydrogel adsorbents. Due to the tendency of MG to readily precipitate in a white form at pH levels above 8, the pH range of MG was limited to 2–8 (Aracier et al. 2021). The solution pH of MB was varied from 2 to 10. The effect of initial dye solutions pH on H-SG/BT(AA/AAm) adsorbing MB and MG as shown in Fig. 5e. The minimum adsorption capacity of MB and MG by H-SG/BT(AA/AAm) were 33 mg/g and 73 mg/g at pH 2, respectively, with removal efficiencies of 17% and 36%. This phenomenon may be attributed to the protonation of $–NH_2$, $–COO^-$, –OH groups at the hydrogel surface, leading to electrostatic repulsion with the cationic dye molecules (Hua et al. 2023). According to the results of pH on the swelling behavior of hydrogels, a large amount of H^+ in the environment formed intramolecular hydrogen bonds with $–COO^-$ groups, resulted in lower swelling ratios and a decline of the contact active sites on H-SG/BT(AA/AAm) surface, ultimately causing a decrease in the adsorption capacity.

The adsorption capacity of H-SG/BT(AA/AAm) for MB (33–181 mg/g) and MG (72–189 mg/g) significantly increased with increasing the pH from 2 to 4. This was attributed to the deprotonation of –COOH and $–NH_3^+$ groups in the H-SG/BT(AA/AAm), which led to an increased number of negatively charged surface binding sites for the adsorption of cationic MB and MG molecules. It was observed that the adsorption capacity of H-SG/BT(AA/AAm) for MB and MG no longer exhibited significant changes with pH when pH > 4. In the pH range of 8–10, the adsorption capacity of MB on H-SG/BT(AA/AAm) decreased slightly, because of the neutralization reaction between –COOH and NaOH in the hydrogel prompted soluble sodium acrylate along the hydrogel chains. Besides, the augmentation of ionized Na^+ would diminish the dissimilarity in permeation between H-SG/BT(AA/AAm) and dye molecules, impeding the ingress of MB molecules into the hydrogel. Furthermore, the intensified competition between Na^+ ions and active cationic groups within MB molecules resulting in adsorption capacity declined.

The pH of the solution reached equilibrium after adsorbing MB and MG are depicted in Fig. 5f. The pHpzc value of H-SG/BT(AA/AAm) is 6.18, indicating that the adsorbent possesses a negative surface charge at pH > 6.18. Specifically, the H-SG/BT(AA/AAm) exhibited an equilibrated pH higher than 6.18 for MB (within pH 5–10) and MG (within pH 6–8). It has been speculated that an electrostatic interaction between the hydrogel and MB/MG molecules facilitating the removal of cationic dyes. The H-SG/BT(AA/AAm) exhibited the highest adsorption capacities for MB and MG at pH 5 and 4, respectively. Moreover, the equilibrium pH values closely resemble those found in natural water, eliminating the need for any adjustments before the dye adsorption process, indicating that the H-SG/BT(AA/AAm) certainly has practical applications.

Effect of Ionic Strength on MB and MG Adsorption

The dye wastewater containing a certain concentration of sodium chloride can improve homogenization during the dyeing process. To simulate the coexisting ions in dye wastewater thereby introducing sodium salt, its effect on adsorbing MB and MG was explored by altering the NaCl concentration. As shown in Fig. 5g, the mass concentration of NaCl of 0–1 wt% had a significant negative impact on adsorption capacity of MB (decreased from 183 to 118 mg/g) and MG (decreased from 177 to 63 mg/g) by H-SG/BT(AA/AAm). This was because that as the NaCl mass content rose, Na^+ ions in the solution competed with the MB and MG for adsorption sites on H-SG/BT(AA/AAm). These Na^+ ions also form complexes by cross-linking with carboxyl groups within the hydrogel. Furthermore, the ion addition reduced the internal osmotic pressure of the hydrogel, making it lower than the external osmotic pressure. It has been reported that the cations can occupy the anion active sites on the hydrogel's surface as the ionic strength elevates (Tasdelen et al. 2022). Higher ionic strength causes a reduction in the adsorption capacities of the hydrogel. Also, the shielding effect resulting from high ionic strength diminishes the MB and MG adsorption capacities on the hydrogel (Melo et al. 2018; Sharma et al. 2022). The findings confirm that electrostatic interactions play an important role in the

adsorption process between the adsorbent and adsorbate, aligning with the experimental observations regarding pH values. Consequently, the H-SG/BT(AA/AAm) exhibited a positive adsorption phenomenon, which made it potentially advantageous in high-salinity effluent treatment.

Effect of Temperature on MB and MG Adsorption

The temperature of the dye solution is a critical determinant of the adsorption capacity and yield, as it influences the rate at which dye molecules move. The effect of temperature on the adsorption behavior of MB and MG by H-SG/BT(AA/AAm) is illustrated in Fig. 5h. Upon examination of the graph, it is evident that the adsorption capacities of MB and MG on H-SG/BT(AA/AAm) demonstrate a negative correlation for MB and a positive correlation for MG with temperature within the range of 25–65 °C. This trend can be attributed to the diminishing interactions between H-SG/BT(AA/AAm) and the solvent as the temperature rises. Additionally, the number of available adsorption sites increases with temperature, which in turn boosts the adsorption capacity of the hydrogel. Also, the increased thermal motion of dye molecules at higher temperatures can enhance migration and diffusion rates, further increasing the adsorption capacity. However, higher temperatures may also lead to desorption of dye molecules from the hydrogel surface, this depending on the binding affinity of the dye molecules to the H-SG/BT(AA/AAm). Compared to MB, MG exhibits a more robust binding affinity with the H-SG/BT(AA/AAm), resulting in a higher propensity for adsorption and consequently a higher adsorption capacity for MG. In contrast, MB is more prone to desorption, causing its adsorption capacity to decrease. Considering the mechanical strength of the hydrogel decreases and its internal structure changes with higher temperatures, and the economic cost in practical applications also increases (Shaki 2023). The adsorption process of MB and MG by the hydrogel was conducted at a temperature of 25 °C.

Adsorption Isotherm and Kinetics Analysis of MB and MG Adsorption

Langmuir and Freundlich models are particularly suitable to recognized the adsorbate-adsorbent interactions. Therefore, the parameters fitted by the Langmuir and Freundlich adsorption isotherm models are presented in Table 1. The Langmuir model exhibited higher correlation coefficients (R^2) for adsorbing MB and MG on H-SG/BT(AA/AAm) compared to the Freundlich model. Specifically, the R^2 values of the Langmuir model were 0.993 for MB and 0.992 for MG, higher than the Freundlich model (0.800 for MB and 0.875 for MG). The maximum experimental adsorption capacities of MB and MG on H-SG/BT(AA/AAm) were 1226 mg/g and 783 mg/g, respectively. These values were closer to the q_m values obtained from the Langmuir model (1250 mg/g for MB and 833 mg/g for MG). Therefore, it can be concluded that the adsorption processes of both MB and MG on H-SG/BT(AA/AAm) better conform to the Langmuir model, indicating a monolayer adsorption on the adsorbent surface with no further uptake upon reaching saturation. Furthermore, the K_L values of the Langmuir model changed between 0 and 1. MB exhibited superior adsorption efficiency on H-SG/BT(AA/AAm) compared to MG, as indicated by the higher K_L values (0.19 for MB and 0.03 for MG) (Ben et al. 2020). Both MB and MG have 1/n values of Freundlich model consistently less than 1, verify that the adsorption processes of MB and MG on H-SG/BT(AA/AAm) were favorable in chemical process and easily implemented (Wang et al. 2023a, b, c). The 1/n value of MB on H-SG/BT(AA/AAm) (0.46) was lower than that of MG (0.52), indicating that more favorable adsorption of MB by H-SG/BT(AA/AAm). These results support the notion that electrostatic attraction is active for the adsorption of dyes within the hydrogel.

Adsorption kinetics, an essential method for predicting adsorption behavior and rates, was utilized to explore the adsorption mechanism of MB and MG molecules onto H-SG/BT(AA/AAm). Table 2 displays the fitting parameters of the adsorption kinetics. The correlation coefficients (R^2) of the pseudo-first-order model were below 0.95 for both MB and MG adsorption on H-SG/BT(AA/AAm), while the R^2 values of the pseudo-second-order model were all above 0.95. Additionally, the adsorption capacities calculated from the pseudo-second-order model ($MB_{qe,\ cal} = 1250$ mg/g, $MG_{qe,\ cal} = 833$ mg/g) were in better agreement with the experimental adsorption capacities ($MB_{qe,\ exp} = 1116$ mg/g, $MG_{qe,\ exp} = 783$ mg/g). Therefore, the adsorption process of MB and MG on H-SG/BT(AA/AAm) followed the pseudo-second-order kinetic model, indicating that chemisorption played a dominant role in the adsorption behavior (Jiang et al. 2023).

To investigate the diffusion of MB and MG molecules into the pores of H-SG/BT(AA/AAm), the parameters of

Table 1 Linear fitting parameters of the adsorption isotherm model for MB and MG adsorption on H-SG/BT(AA/AAm)

Dyes	Langmuir model			Freundlich model			$q_{m,exp}$/(mg/g)
	K_L/(L/mg)	$q_{m,cal}$/(mg/g)	R^2	K_f/(mg/g)	1/n	R^2	
MB	0.19	1250	0.992	215	0.46	0.800	1226
MG	0.03	833	0.993	44	0.52	0.875	783

Table 2 Fitting parameters of adsorption kinetic models of MB and MG adsorption on H-SG/BT(AA/AAm)

Dyes (mg/L)	Pseudo-first order kinetic model			Pseudo-second order kinetic model			Intra-particle diffusion model			$q_{m,exp}$/(mg/g)
	$k_1 \times 10^{-4}$/min^{-1}	$q_{e,cal}$/(mg/g)	R^2	$k_2 \times 10^{-4}$/(g/mg min)	$q_{e,cal}$/(mg/g)	R^2	K_1	K_2	K_3	
MB										
100	12.0	114	0.713	0.366	200	0.995	7.85	0.73	0.21	191
600	17.0	719	0.855	0.037	1250	0.996	44.79	4.87	0.25	1116
MG										
100	10.0	158	0.898	0.180	213	0.999	7.02	2.85	0.69	192
600	12.0	558	0.824	0.046	833	0.997	28.88	12.81	1.47	783

intra-particle diffusion model are also given in Table 2. The adsorption-diffusion process can be divided into three segments: external film diffusion, intra-particle diffusion, and surface adsorption. Analysis of the fitting results using the intra-particle diffusion model revealed that the rate constants for these segments followed the order $K_1 > K_2 > K_3$. This suggests that the adsorption process involved surface adsorption initially, followed by rapid intra-particle diffusion, and finally concluded with a slower intra-particle diffusion process (Lu et al. 2022). The surface adsorption segment of H-SG/BT(AA/AAm) exhibited a rapid adsorption rate, higher than the subsequent two segments. In conclusion, the film diffusion mainly governed the rate-limiting adsorption process for MB and MG onto H-SG/BT(AA/AAm).

Thermodynamic Analysis of MB and MG Adsorption

Thermodynamic study determines whether adsorption is spontaneous, quantify its thermodynamic tendency, and identify the dominant adsorption model. Therefore, the values of ΔH, ΔS, and ΔG were also calculated, and the obtained values are listed in Table 3. It can be seen that all ΔG values were negative, indicating that the adsorption of MB and MG by H-SG/BT(AA/AAm) was spontaneous. The negative value of ΔH (− 14.51 kJ/mol) demonstrated the exothermic essence of MB adsorption on H-SG/BT(AA/AAm), suggesting that the heating is not conducive to MB adsorption. The negative value of ΔS (− 21.18 J/mol K) verified that the orderliness of whole solution system increased after MB adsorbed. Whereas, positive value of ΔH (29.87 kJ/mol) confirmed the endothermic process of MG adsorption on H-SG/BT(AA/AAm). The differences in MB and MG adsorption on H-SG/BT(AA/AAm) can be attributed to temperature effects. As the temperature increases, dye molecules have enhanced diffusion capacity but reduced surface tension with the hydrogel, leading to a decrease in dye adsorption capacity. However, temperature also promotes hydrogel swelling, creating additional adsorption sites and increasing the binding rate of dye molecules. MB, being smaller in size, can more easily penetrate the hydrogel's interior, resulting in a higher adsorption capacity compared to MG. Additionally, the change in dye molecules also impacts the solution environment, contributing to the distinct adsorption thermodynamics observed in the experiments conducted by Liu et al. (2019). The positive value of ΔS (121.73 J/mol K) signifies an increase in entropy, reflecting a state of disorder at the solid–liquid interface (Banisheykholeslami et al. 2021). The adsorption process is associated with physical adsorption (hydrogen bonding and Van der Waals forces) when ΔH varies between 2 and 10 kJ/mol, whereas higher ΔH (> 40 kJ/mol) represents the chemisorption (Mahmoud et al. 2021; Abuhatab et al. 2020). The ΔH of MB and MG adsorption on H-SG/BT(AA/AAm) was 14.51 kJ/mol and 29.87 kJ/mol, respectively. It is noteworthy that the adsorption process may potentially encompass various reaction pathways (such as ion exchange, hydrogen bonds, and electrostatic attraction).

Reusability Analysis of H-SG/BT(AA/AAm)

Regeneration and reutilization of adsorbents are crucial for their potential commercial applications. Therefore, an adsorption–desorption experiment with H-SG/BT(AA/AAm) was also conducted. A notable advantage of H-SG/BT(AA/AAm) is its quick separability from the solution

Table 3 Thermodynamic adsorption parameters of H-SG/BT(AA/AAm)

Dyes	ΔH (kJ/mol)	ΔS (J/mol K)	ΔG (kJ/mol)					R^2
			298 K	308 K	318 K	328 K	338 K	
MB	− 14.51	− 21.18	− 8.19	− 7.99	− 7.77	− 7.56	− 7.35	0.991
MG	29.87	121.73	− 6.41	− 7.62	− 8.84	− 10.06	–11.27	0.981

without the need for any additional tools. According to the results of pH experiments, the adsorption capacity of MB and MG on H-SG/BT(AA/AAm) was sensitive to low pH levels. Also, the H^+ ions in HCl can react with the negatively charged functional groups (such as COO^-) on the hydrogel, thereby eliminating the attraction of these functional groups to the cationic dyes MB and MG (Poornachandhra et al. 2023). Relevant literature has reported that HCl, when used as the eluent in desorption experiments, has demonstrated a high desorption rate (Jana et al. 2019). Therefore, 0.1 mol/L HCl was used as desorption solution for reusing the adsorbent.

The adsorption–desorption results of the H-SG/BT(AA/AAm) after adsorbing MB and MG are depicted in Fig. 6. In the experiment, the hydrogel was added to the contaminant solution, and after reaching adsorption saturation, it was regenerated using a 0.1 mol/L HCl eluent. Over five cycles, the adsorption efficiency of H-SG/BT(AA/AAm) for MB declined by 12%, dropping from 93 to 81% (Fig. 6b). Likewise, the efficiency for MG fell by 6%, from 90 to 84%, over the same cycles (Fig. 6c). The reduced adsorption performance is attributed to repulsion between the positively charged MB and MG molecules and the protonated hydrogel surface in an acidic medium (Vaid et al. 2023). Besides, some of the residual dye being adsorbed on the adsorbent surface, the gradual blockage of the active sites and the inevitable loss of adsorbents during the desorption recovery process also caused the decline in activity of H-SG/BT(AA/AAm) for MB and MG after reuse (Li et al. 2019a, b; Uko et al. 2022; Benamer-Oudih et al. 2023). The desorption efficiency of the H-SG/BT(AA/AAm) for MB declined by 7% (from

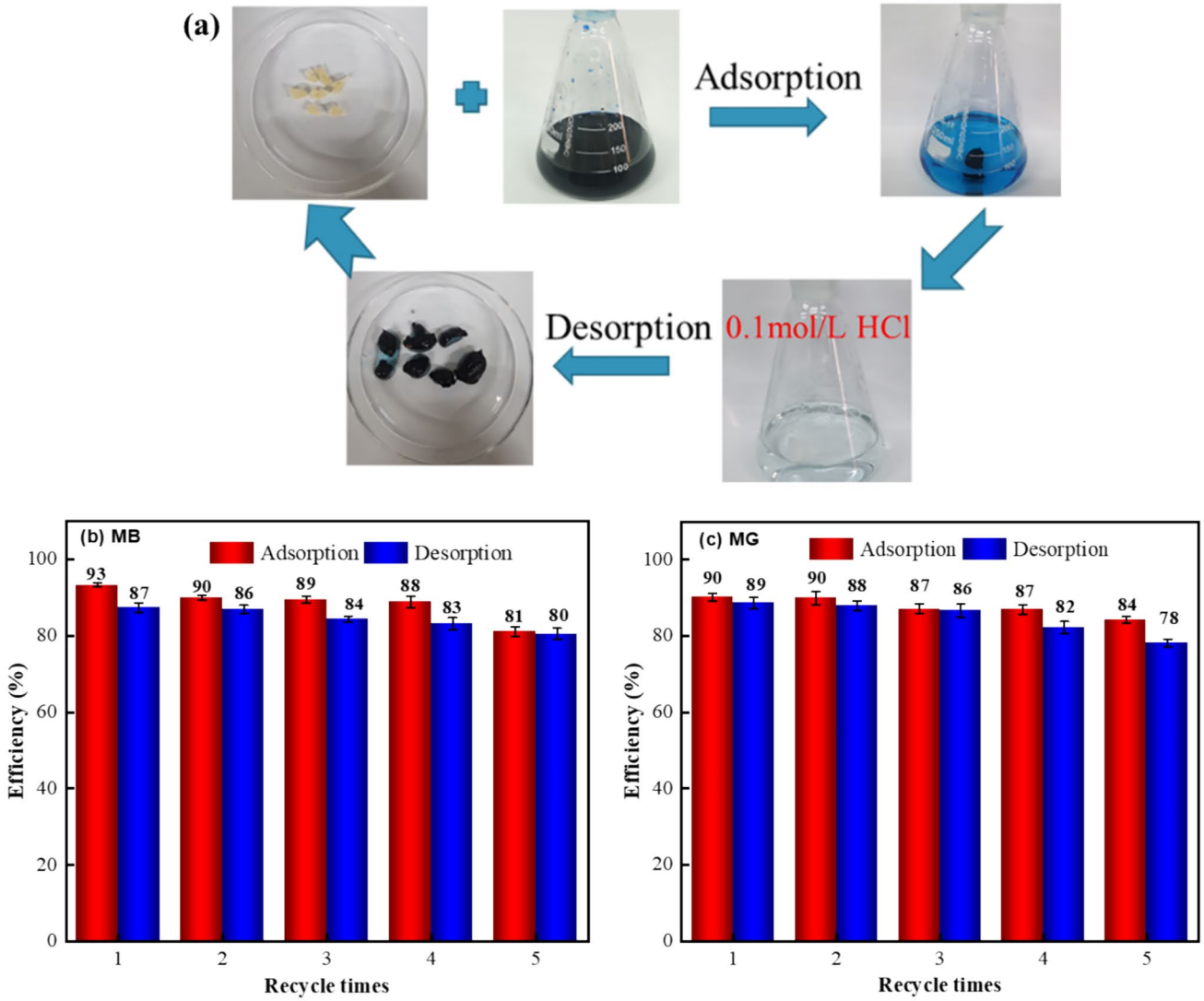

Fig. 6 Adsorption–desorption process of H-SG/BT(AA/AAm) (**a**); reusability test of H-SG/BT(AA/AAm) for MB (**b**) and MG (**c**) adsorption

87 to 80%), and for MG, it fell by 12% (from 89 to 78%). These declines confirm that the HCl eluent was effective for desorption, maintaining consistent performance. After five adsorption–desorption cycles, the removal efficiency for both MB and MG remained at 80%, suggesting that H-SG/BT(AA/AAm) has favorable cycling behavior.

Adsorption Mechanism

To further explore the adsorption mechanisms of MB and MG dyes on H-SG/BT(AA/AAm), the materials were characterized using FT-IR and SEM–EDS analyses before and after adsorption. As shown in Fig. 7, the peaks at 1599 cm^{-1} and 1395 cm^{-1} were assigned with aromatic bonds, while peaks at 884 cm^{-1} and 665 cm^{-1} corresponded to C–H bending and C–S–C stretching vibrations, respectively (Chen et al. 2022). These adsorption peaks were observed after MB adsorption, confirming the adsorption of MB on hydrogel (Fig. 7a). Post-adsorption MG, a characteristic absorption peak of aromatic skeleton C=C at 1587 cm^{-1} was observed. A new peak at 1171 cm^{-1} assigning phenyl ring C–N stretching vibration of MG was also identified (Fig. 7b) (Vaid et al. 2023). Moreover, a broad absorption peak at 3456 cm^{-1} shifted plainly to the vicinity of 3445 cm^{-1} after the adsorption of MB and MG. The observed shift in –OH and N–H vibration peaks to lower wavenumbers suggests that the hydroxyl and amine groups of t H-SG/BT(AA/AAm) could potentially interact with MB and MG molecules through hydrogen bonding (Khan et al. 2023). Apart from that, the peaks at 1658 cm^{-1}, 1560 cm^{-1}, and 1456 cm^{-1}

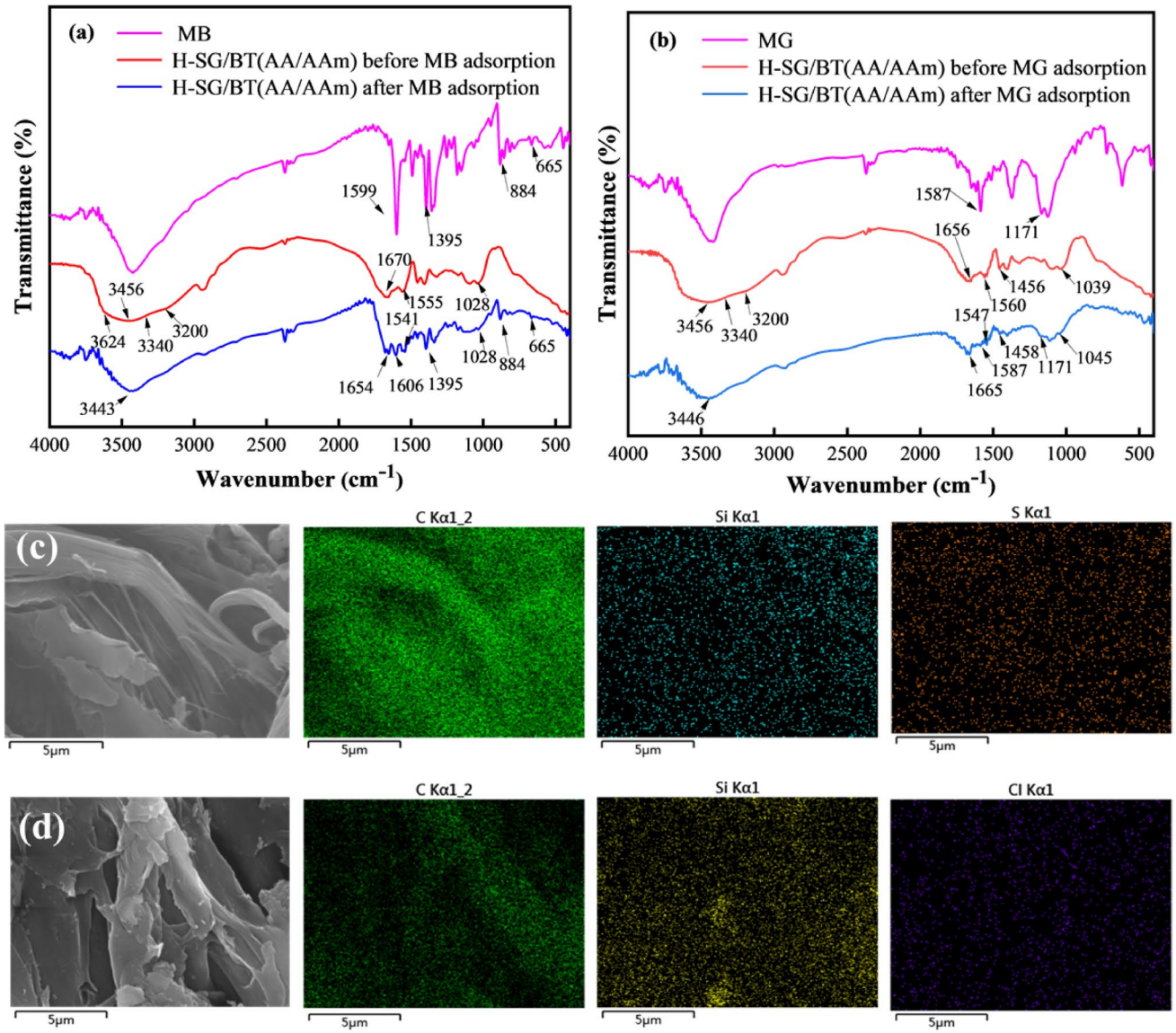

Fig. 7 FTIR and SEM–EDS images of H-SG/BT(AA/AAm) before and after MB (**a**, **c**), MG (**b**, **d**) adsorption

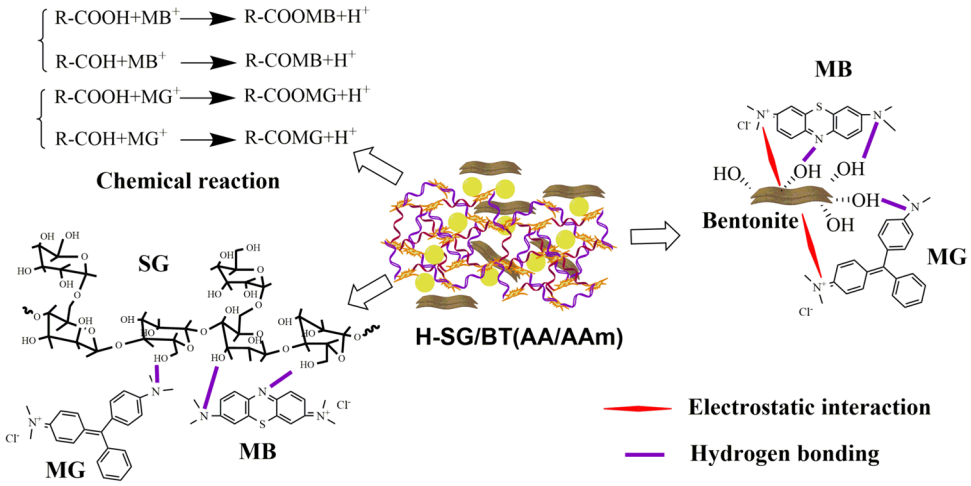

Fig. 8 Possible adsorption mechanism of MB and MG by H-SG/BT(AA/AAm)

ascribed to –COO– stretching vibration peaks were subsided and shifted to 1654–1665 cm^{-1}, 1547–1562 cm^{-1} and 1455–1458 cm^{-1}, respectively. These changes signify that the –COOH functional groups may engage in electron transfer with nitrogen atoms in MB and MG molecules, leading to the formation of chemical bonds.

The SEM and EDS images of H-SG/BT(AA/AAm) post-adsorption of MB and MG are observed in Fig. 7c, d. With molecular formulas of $C_{16}H_{18}ClN_3S$ for MB and $C_{23}H_{25}ClN_2$ for MG, the distinctive elements S and Cl can be used to identify whether the dyes are adsorbed onto the hydrogel. Therefore, the uniform distribution of S and Cl elements across the hydrogel surface suggests that MB and MG have been successfully adsorbed onto H-SG/BT(AA/AAm). Compared with H-SG/BT(AA/AAm), the pore diameter was observed to decrease after the adsorption of MB and MG, with some porosity still evident on the surface. This reduction was attributed to the electrostatic interaction between the positively charged dyes and the negatively charged carboxyl groups (–COOH) present on the hydrogel. Moreover, due to their macromolecular nature, the dyes can obstruct the pores during the adsorption process, contributing to the observed decrease in adsorbent pore size.

From the FTIR and SEM–EDS results, the –OH, –COOH, and $–NH_2$ groups on the H-SG/BT(AA/AAm) surface have shown chemical bond interactions with dye molecules. The SG chains and BT surface, both of which have abundant –OH groups, can interact with $–N(CH_3)_3$ groups in MB and MG molecules through hydrogen bonding. Additionally, the negatively charged BT surface is bonding with cationic groups in the dyes via electrostatic attraction. The pH_{pzc} of H-SG/BT(AA/AAm) was 6.18, and the pH values consistently remained higher than 6.18 after reaching adsorption equilibrium. This indicates that electrostatic interactions significantly contributed to the MB and MG adsorption. According to the kinetic model and thermodynamic study, it was found that the multiple mechanisms (including electrostatic interactions, chemical bonds, and hydrogen bonds) are involved in the dye removal process on H-SG/BT(AA/AAm). In addition, the high porosity and swelling of H-SG/BT(AA/AAm) also favor dye adsorption by facilitating the swift movement of dye molecules. The potential adsorption mechanisms between the hydrogel and dye molecules are depicted in Fig. 8.

Conclusion

The H-SG/BT(AA/AAm) was successfully functionalized by a unique cross-linking agent HPSi with the aim of enhancing mechanical behavior and used for adsorbing MB and MG. It was concluded that the –OH and $–COO^-$ groups of BT, SG and AA/AAm were synergistically immobilized in H-SG/BT(AA/AAm), exhibited a remarkable equilibrium adsorption capacity (1226 mg/g for MB and 783 mg/g for MG), highest removal efficiencies of MB and MG (maintained above 90% at pH 4–8). The main adsorption forces between hydrogels and dyes was chemical bonding, hydrogen bonding, and electrostatic attraction. H-SG/BT(AA/AAm) exhibited good swelling properties and sustainable adsorption capacity for MB and MG, with 86% retention after five reuse cycles and desorption efficiency over 78%. The characterization results of H-SG/BT(AA/AAm) showed that HPSi and BT has refined the porous structure of hydrogel, the tensile strength and rupture work of H-SG/BT(AA/AAm) prepared with HPSi crosslinker were 2.76 and 23.36 times higher than MBAA hydrogel. Adsorption kinetics and isotherms analysis of MB and MG were better fitted with the pseudo-second-order kinetic and Langmuir isotherm models, indicating that monolayer adsorption dominated by chemical adsorption was the primary mechanism. Thermodynamic analysis reflected that the adsorption of MB by H-SG/BT(AA/AAm) was spontaneously feasible and exothermic, while the

adsorption of MG was spontaneously feasible and thermally absorptive. In conclusion, H-SG/BT(AA/AAm) possessed high efficiency in cationic dyes adsorption. Therefore, the multifunctional, biodegradable, highly swollen and resilient H-SG/BT(AA/AAm) can make a significant contribution to industrial dye effluents treatment and can also be utilized as a potential material in controlled-release agricultural fertilizers and pesticides.

Supplementary Information The online version contains supplementary material available at https://doi.org/10.1007/s41742-024-00624-3.

Author contributions Luying Jiang: Investigation, Experiments, Writing-original draft. Sishan Yu: Investigation, Experiments, Writing. Jingwei Zhang: Writing-review & editing. Zisong Xu: Conceptualization, Supervision, Project administration. Rui Tang: Conceptualization, Supervision, Project administration. Yinlong Wang: Investigation, Methodology, Manuscript proofreading. Ke Liang: Mechanical experimental design, data analysis and mechanical performance testing of hydrogel. Chen Zhai: Conceptualization, Supervision, Project administration. Zhangfa Tong: Conceptualization, Resources, Funding acquisition. Hanbing Zhang: Conceptualization, Resources, Funding acquisition.

Funding We would like to acknowledge the financial support provided by the National Science Foundation of China (Grant number 22378084), Guangxi Key Technologies R&D Program (AB22080085), the Cooperative Innovation Project of Guangxi province (CZNF-JSZX20-3), and the Petrochemical Resources Processing and Process Reinforcement Technology Key Laboratory Project of Guangxi province (Grant number 2022Z005). Their support has been instrumental in the successful completion of this work.

Data availability All data generated or analysed during this study are included in this published article [and its supplementary information files].

Declarations

Conflict of interest The authors declare that they have no competing interests regarding the publication of this research article. There are no financial or non-financial interests that could be perceived as potentially influencing the objectivity, integrity, or validity of the research findings presented in this paper.

Ethical approval The submitted work has been carried by adhering to the accepted ethical standards.

Consent to participate The authors give their consent to participate in peer review process.

Consent for publication All the authors give their consent for the publication.

References

Abdel-Bary EM, Elbedwehy AM (2018) Graft copolymerization of polyacrylic acid onto Acacia gum using erythrosine-thiourea as a visible light photoinitiator: application for dye removal. Polym Bull 75:3325–3340. https://doi.org/10.1007/s00289-017-2205-x

Abuhatab S, El-Qanni A, Al-Qalaq H, Hmoudah M, Al-Zerei W (2020) Effective adsorptive removal of Zn^{2+}, Cu^{2+}, and Cr^{3+} heavy metals from aqueous solutions using silica-based embedded with NiO and MgO nanoparticles. J Environ Manag 268:110713. https://doi.org/10.1016/j.jenvman.2020.110713

Aracier ED, Urucu OA, Cakmakci E (2021) Imidazole modified acrylate-containing photocured hydroGels-basel for the efficient removal of malachite green dye from aqueous solutions. J Appl Polym Sci 138:51415. https://doi.org/10.1002/app.51415

Bahaar H, Reddy SG, Kumar BS (2023) Modified layered double hydroxide—PEG magneto-sensitive hydrogels with suitable lignoalginate green polymer composite for prolonged drug delivery applications. Eng Sci 24:914. https://doi.org/10.30919/es914

Banisheykholeslami F, Hosseini M, Darzi GN (2021) Design of PAMAM grafted chitosan dendrimers biosorbent for removal of anionic dyes: adsorption isotherms, kinetics and thermodynamics studies. Int J Biol Macromol 177:306–316. https://doi.org/10.1016/j.ijbiomac.2021.02.118

Bashir S, Teo YY, Ramesh S, Ramesh K, Mushtaq MW (2018) Rheological behavior of biodegradable N-succinyl chitosan-g-poly (acrylic acid) hydroGels-basel and their applications as drug carrier and in vitro theophylline release. Int J Biol Macromol 117:454–466. https://doi.org/10.1016/j.ijbiomac.2018.05.182

Ben AM, Wang FY, Boukherroub R, Xia MZ (2020) High performance of phytic acid-functionalized spherical polyphenylglycine particles for removal of heavy metal ions. Appl Surf Sci 518:146206. https://doi.org/10.1016/j.apsusc.2020.146206

Benamer-Oudih S, Tahtat D, Nacer Khodja A, Mansouri B, Mahlous M, Guittoum AE, Kebbouche Gana S (2023) Sorption behavior of chitosan nanoparticles for single and binary removal of cationic and anionic dyes from aqueous solution. Environ Sci Pollut Res. https://doi.org/10.1007/s11356-023-27907-0

Benhouria A, IslamM A, Zaghouane-Boudiaf H, Boutahala M, Hameed BH (2015) Calcium alginate-bentonite-activated carbon composite beads as highly effective adsorbent for methylene blue. Chem Eng J 170:621–630. https://doi.org/10.1016/j.cej.2015.02.030

Chang KY, Chou YN, Chen WY, ChenC Y, Lin HR (2022) Mussel-inspired adhesive and self-healing hydrogel as an injectable wound dressing. Polymers (basel) 14:3346. https://doi.org/10.3390/polym14163346

Chen YN, Li LS, Li YP, Liu YH, Chen YR, Li H, Li ML, Xu FT, Liu YQ (2022) Preparation of a double-network hydrogel based on wastepaper and its application in the treatment of wastewater containing copper(II) and methylene blue. Rsc Adv 11:18131–18143. https://doi.org/10.1039/d1ra02321g

Chen ZY, Zhang MY, Ren PG, Lan Z, Guo ZZ, Yan HX, Jin YL, Ren F (2023) Enhanced mechanical and tribological properties of epoxy composites reinforced by novel hyperbranched polysiloxane functionalized graphene/ MXene hybrid. Chem Eng J 466:143086. https://doi.org/10.1016/j.cej.2023.143086

Dai HJ, Huang Y, Huang HH (2018) Eco-friendly polyvinyl alcohol/carboxymethyl cellulose hydroGels-basel reinforced with graphene oxide and bentonite for enhanced adsorption of methylene blue. Carbohyd Polym 185:1–11. https://doi.org/10.1016/j.carbpol.2017.12.073

Devkar P, Nangare S, Zawar L, Shirsath N, Bafna P, Jain P (2023) Design of polyacrylamide grafted sesbania gum-mediated pH-responsive IPN-based microbeads for delivery of diclofenac sodium: In-vitro-in-vivo characterizations. Int J Biol Macromol 230:123360. https://doi.org/10.1016/j.ijbiomac.2023.123360

Du J, Xu SM, Feng S, Yu L, Wang JD, Liu YM (2016) Tough dual nanocomposite composite hydrogels with inorganic hybrid crosslinking. Sofa Matter 12:1649–1654. https://doi.org/10.1039/C5SM02790J

Elsaeed SM, Zaki EG, Abdelhafes A, Al-Hussaini AS (2022) Response surface method based modeling and optimization of CMC-g

terpolymer interpenetrating network/bentonite superabsorbent composite for enhancing water retention. ACS Omega 7:8219–8228. https://doi.org/10.1021/acsomega.1c03194

Flores-Cespedes F, Villafranca-Sanchez M, Fernandez-Perez M (2023) Alginate-bentonite-based hydrogels-basel designed to obtain controlled-release formulations of dodecyl acetate. Gels 9:388. https://doi.org/10.3390/Gels-basel9050388

Ghadami A, Taheri S, Alinejad Z, Dinari M (2022) Preparation of acrylate-based double and triple interpenetrating polymer networks hydroGels-basel: rheological, thermal, and swelling behavior. Polym Advan Technol 33:4330–4340. https://doi.org/10.1002/pat.5862

Ghafelebashi A, Khosravani S, Kazemi MH, Rajabi F, Amiri MC (2018) A novel fabricated polyvinyl alcohol/bentonite nanocomposite hydrogel generated into colloidal gas aphron. Colloid Surface A 650:129580. https://doi.org/10.1016/j.colsurfa.2022.129580

Ghumman SA, Noreen S, Hameed H, Elsherif MA, Shabbir R, Rana M, Junaid K, Bukhari SNA (2022) Synthesis of pH-sensitive cross-linked basil seed gum/acrylic acid HydroGels-basel by free radical copolymerization technique for sustained delivery of captopril. Gels 8:291. https://doi.org/10.3390/Gels-basel8050291

Hooshvar M, Marandi GB, Nakhjiri MT (2024) Collagen-based hydrogel nanocomposite as adsorbent for methylene blue and crystal violet removal from aqueous solution: isotherm, kinetic, and thermodynamic studies. Water Air Soil Pollut. https://doi.org/10.1007/s11270-024-06971-3

Hua YW, Xu DH, Liu ZX, Zhou J, Han JT, Lin ZH, Xu D, Chen G, Huang XD, Chen J, Lv J, Liu GY (2023) Effective adsorption and removal of malachite green and Pb^{2+} from aqueous samples and fruit juices by pollen–inspired magnetic hydroxyapatite nanoparticles/hydrogel beads. J Clean Prod 411:137233. https://doi.org/10.1016/j.jclepro.2023.137233

Jana S, Ray J, Mondal B, Tripathy T (2019) Efficient and selective removal of cationic organic dyes from their aqueous solutions by a nanocomposite hydrogel, katira gum-cl-poly(acrylic acid-co-N, N-dimethylacrylamide)@bentonite. Appl Clay Sci 173:46–64. https://doi.org/10.1016/j.clay.2019.03.009

Jiang MW, Niu N, Chen LG (2022) A template synthesized strategy on bentonite-doped lignin hydrogel spheres for organic dyes removal. Sep Purif Technol 285:120376. https://doi.org/10.1016/j.seppur.2021.120376

Jiang MH, Simayi R, Sawutu A, Wang JX, Wu TX, Gong XK (2023) Modified β-Cyclodextrin hydrogel for selective adsorption and desorption for cationic dyes. Colloid Surf A 661:130912. https://doi.org/10.1016/j.colsurfa.2022.130912

Khan SA, Siddiqui MF, Khan TA (2020) Ultrasonic-assisted synthesis of polyacrylamide/bentonite hydrogel nanocomposite for the sequestration of lead and cadmium from aqueous phase: equilibrium, kinetics and thermodynamic studies. Ultrason Sonochem 60:104761. https://doi.org/10.1016/j.ultsonch.2019.104761

Khan SA, Rehman TU, Shah LA, Ullah M (2023) Magnetite graphene oxide-doped superadsorbent hydrogel for efficient removal of crystal violet from wastewater. Chem Pap 77:2725–2735. https://doi.org/10.1007/s11696-023-02662-1

Khatooni H, Peighambardoust SJ, Foroutan R, Mohammadi R, Ramavandi B (2023) Adsorption of methylene blue using sodium carboxymethyl cellulose-g-poly (acrylamide-co-methacrylic acid)/Cloisite 30B nanocomposite hydrogel. J Polym Environ 31:297–311. https://doi.org/10.1007/s10924-022-02623-x

Lan S, Lu YN, Zhang JH, Guo YA, Li C, Zhao S, Sheng XL, Dong A (2019) Electrospun sesbania gum-based polymeric N-halamines for antibacterial applications. Polymers 11:1117. https://doi.org/10.3390/polym11071117

Li SN, Li BQ, Gong LX, Yu ZR, Feng YJ, Jia DC, Zhou Y, Tang LC (2019a) Enhanced mechanical properties of polyacrylamide/chitosan hydroGels-basel by tuning the molecular structure of hyperbranched polysiloxane. Mater Des 162:162–170. https://doi.org/10.1016/j.matdes.2018.11.045

Li ZC, Wang YH, Zheng S, Qian P, Zhang XM, Han PW, Tu YB, Ye SF (2019b) Nanosheets−MnxOy anchored biochar for efficient removal of methyl blue and tetracycline from water. Chem Eng Res Des 182:13–24. https://doi.org/10.1016/j.cherd.2022.03.032

Li B, Hao WR, Xu XJ, Liu JZ, Fu DD, Zhou MJ, Hu ZG (2023) Preparation and properties of P(IA-co-AA-co-AM) composite hydrogel via frontal polymerization. Colloid Polym Sci 301:445–453. https://doi.org/10.1007/s00396-023-05079-0

Liu WY, Wang TY, Wang CY, Bi CC, Liu M, Yu H (2019) Study of adsorption performance of cationic dyes methylene blue and malachite green by poly (acrylate-co-acrylamide) hydrogel. Chin J Anal Chem 47:1785–1793. https://doi.org/10.19756/j.issn.0253-3820.191255

Lu XH, Zhou XQ, Qiu W, Wang ZY, Wang YS, Zhang HC, Yu JX, Wang D, Gu J, Ma J (2022) Kinetics and mechanism of the reaction of hydrogen peroxide with hypochlorous acid: Implication on electrochemical water treatment. J Hazard Mater 438:129420. https://doi.org/10.1016/j.jhazmat.2022.129420

Mahmoud ME, Amira MF, Azab MM, Abdelfattah AM (2021) Effective removal of levofloxacin drug and Cr(VI) from water by a composed nanobiosorbent of vanadium pentoxide@chitosan@MOFs. Int J Biol Macromol 188:879–891. https://doi.org/10.1016/j.ijbiomac.2021.08.092

Mamytbekov GK, Zheltov DA, Nurtazin YR (2023) Synthesis and investigation of the properties of biphasic hybrid composites based on bentonite, copper hexacyanoferrate acrylamide and acrylic acid hydrogel. Polymers 15:2586. https://doi.org/10.3390/polym15122586

Matsuda T, Nakajima T, Gong JP (2019) Fabrication of tough and stretchable hybrid double-network elastomers using ionic dissociation of polyelectrolyte in nonaqueous media. Chem Mater 31:3766–3776. https://doi.org/10.1021/acs.chemmater.9b00871

Melendez-Ortiz HI, Betancourt-Galindo R, Puente-Urbin B, Ledezma A, Rodríguez-Fernández O (2022) Synthesis and characterization of hydroGels basel based on maltodextrins with antimicrobial properties. Int J Polym Mater 71:959–968. https://doi.org/10.1080/00914037.2021.1931209

Melo BC, Paulino FAA, Cardoso VA (2018) Cellulose nanowhiskers improve the methylene blue adsorption capacity of chitosan-g-poly(acrylic acid) hydrogel. Carbohyd Polym 181:358–367. https://doi.org/10.1016/j.carbpol.2017.10.079

Mokhtar A, Abdelkrim S, Sardi A, Benyoub A, Besnaci H, Cherrak R, Hadjel M, Boukoussa B (2020) Preparation and characterization of anionic composite hydrogel for dyes adsorption and filtration: non-linear isotherm and kinetics modeling. J Polym Environ 28:1710–1723. https://doi.org/10.1007/s10924-020-01719-6

Myint TT, Ge JG, Niu HJY, Chen J, Jiao Z (2020) A separation-free and pizza-structure PAM/GCN/PAA composite hydrogel (PCH) in wastewater treatment at visible light or solar light. Sci Total Environ 705:135821. https://doi.org/10.1016/j.scitotenv.2019.135821

Njuguna DG, Schönherr H (2022) Smart and regeneratable Xanthan gum hydrogel adsorbents for selective removal of cationic dyes. J Environ Chem Eng 10:107620. https://doi.org/10.1016/j.jece.2022.107620

Ozsoy F, Ozdilek B, Onder A, Ilgin P, Ozay H, Ozay O (2022) Graphene nanoplate incorporated Gelatin/poly(2-(Acryloyloxy) ethyl trimethylammonium chloride) composites hydrogel for highly effective removal of Alizarin Red S from aqueous solution. J Polym Res 29:11. https://doi.org/10.1007/s10965-022-03327-5

Pandey S (2017) A comprehensive review on recent developments in bentonite-based materials used as adsorbents for wastewater

treatment. J Mol Liq 241:1091–1113. https://doi.org/10.1016/j.molliq.2017.06.115
Pandey S, Makhado E, Kim S, Kang M (2023) Recent developments of polysaccharide based superabsorbent nanocomposite for organic dye contamination removal from wastewater—a review. Environ Res 217:114909. https://doi.org/10.1016/j.envres.2022.114909
Pereira KAB, Aguiar KLNP, Oliveira PF, Vicente BM, Pedroni LG, Mansur CRE (2020) Synthesis of hydrogel nanocomposites based on partially hydrolyzed polyacrylamide, polyethyleneimine, and modified clay. ACS Omega 5:4759–4769. https://doi.org/10.1021/acsomega.9b02829
Poornachandhra C, Jayabalakrishnan RM, Prasanthrajan M, Balasubramanian G, Lakshmanan A, Selvakumar S, John JE (2023) Cellulose-based hydrogel for adsorptive removal of cationic dyes from aqueous solution: isotherms and kinetics. RSC Adv 13(7):4757–4774. https://doi.org/10.1039/D2RA08283G
Ren LR, Li WJ, Zhang DQ, Fang WS, Yan DD, Wang QX, Jin X, Li Y, Cao AC (2023) Silica modified copper-based alginate/chitosan hybrid hydrogel to control soil fumigant release, reduce emission and enhance bioactivity. Int J Biol Macromol 244:125132. https://doi.org/10.1016/j.ijbiomac.2023.125132
Saigl Z, Tifouti O, Alkhanbashi B, Alharbi G, Algamdi H (2023) Chitosan as adsorbent for removal of some organic dyes: a review. Chem Pap 77:2363–2405. https://doi.org/10.1007/s11696-022-02641-y
Santoso SP, Kurniawan A, Angkawijaya AE, Shuwanto H, Warmadewanthi IDA, Hsieh CW, Hsu HY, Soetaredjo FE, Ismadji S, Cheng KC (2023) Removal of heavy metals from water by macro-mesoporous calcium alginate-exfoliated clay composite sponges. Chem Eng J 452:139261. https://doi.org/10.1016/j.cej.2022.139261
Sekine Y, Nakawa T, Yunoki SJ, Sugita T, Nakagawa H, Yamada T (2020) Eco-friendly carboxymethyl cellulose nanofiber composite hydrogels prepared via freeze cross-linking and their applications. ACS Appl Polym Mater 2:5482–5491. https://doi.org/10.1021/acsapm.0c00831
Shaki H (2023) The removal of methylene blue and maxilon blue dyes using a polyvinyl alcohol/poly(acrylic acid-co-acrylamide) composite hydrogel from water. Pigm Resin Technol 52:521–531. https://doi.org/10.1108/PRT-11-2021-0130
Shao Y, Zhu Y, Zheng R, Wang P, Zhao Z, An J (2022) Highly sensitive and selective surface molecularly imprinted polymer electrochemical sensor prepared by Au and MXene modified glassy carbon electrode for efficient detection of tetrabromobisphenol A in water. Adv Compos Hybrid Mater 5(4):3104–3116. https://doi.org/10.1007/s42114-022-00562-8
Sharma V, Kumar V, Choudhary S, Sharma K (2022) Performance evaluation of gum Gellan-based hydrogel as a novel adsorbent for the removal of cationic dyes: linear regression models. ACS Appl Mater Interfaces 300:785–800. https://doi.org/10.1021/acsami.2c20710
Shi Y, Li B, Jiang X, Yu C, Li T, Sun H, Chen S, Li D, Sun D (2023) In situ enhancing thermal and mechanical properties of novel green WPAI nanocomposite membrane via artificially cultivated biomass-based diatom frustules. Adv Compos Hybrid Mater 6(1):36. https://doi.org/10.1007/s42114-022-00621-0
Shirsath SR, Hage AP, Zhou M, Sonawane SH, Ashokkumar M (2011) Ultrasound assisted preparation of nanoclay Bentonite-FeCo nanocomposite hybrid hydrogel: a potential responsive sorbent for removal of organic pollutant from water. Desalination 281:429–437. https://doi.org/10.1016/j.desal.2011.08.031
Sidheekha MP, Shabeeba A, Rajan L, Thayyil MS, Ismail YA (2023) Conducting polymer/hydrogel hybrid free-standing electrodes for flexible supercapacitors capable of self-sensing working conditions: large-scale fabrication through facile and low-cost route. Eng Sci 23:890. https://doi.org/10.30919/es890
Tang HB, Liu YH, Li YP, Li Q, Liu XJ (2020) Hydroxypropylation of cross-linked sesbania gum, characterization and properties. Int J Biol Macromol 152:1010–1019. https://doi.org/10.1016/j.ijbiomac.2019.10.188
Tasdelen B, Cifci DI, Meric S (2022) Preparation and characterization of chitosan/AMPS/kaolinite composite hydroGels-basel for adsorption of methylene blue. Polym Bull 79:9643–9662. https://doi.org/10.1007/s00289-021-03970-w
Uko CA, Tijani JO, Abdulkareem SA, Mustapha S, Egbosiuba TC, Muzenda E (2022) Adsorptive properties of MgO/WO_3 nanoadsorbent for selected heavy metals removal from indigenous dyeing wastewater. Process Saf Environ 162:775–794. https://doi.org/10.1016/j.psep.2022.04.057
Vaid V, Khushbu K, Kaur K, Bansal A, Panwar A, Devi A (2023) Removal of organic dyes from aqueous solutions by adsorption of chitosan-guar gum-based glyoxal crosslinked hydrogel. Fiber Polym 24:383–401. https://doi.org/10.1007/s12221-023-00080-4
Wang WB, Wang AQ (2010) Nanocomposite of carboxymethyl cellulose and attapulgite as a novel pH-sensitive superabsorbent: synthesis, characterization and properties. Carbohyd Polym 82:83–91. https://doi.org/10.1016/j.carbpol.2010.04.026
Wang LZ, Yu GB, Li JC, Feng YH, Peng Y, Zhao XY, Tang YY, Zhang Q (2019) Stretchable hydrophobic modified alginate double-network nanocomposite hydroGels-basel for sustained release of water-insoluble pesticides. J Clean Prod 226:122–132. https://doi.org/10.1016/j.jclepro.2019.03.341
Wang LY, Wang Y, Li XY, He TT, Wang R, Zhao Y, Song H, Wang H (2021) 3D/2D Fe_2O_3/g-C_3N_4 Z-scheme heterojunction catalysts for fast, effective and stable photo Fenton degradation of azo dyes. J Environ Chem Eng 9:105907. https://doi.org/10.1016/j.jece.2021.105907
Wang XC, Hou XJ, Zou PY, Huang AM, Zhang M, Ma L (2022) Cationic starch modified bentonite-alginate nanocomposites for highly controlled diffusion release of pesticides. Int J Biol Macromol 213:123–133. https://doi.org/10.1016/j.ijbiomac.2022.05.148
Wang B, Kuang Y, Li M, Wang X, Zhang X, Rao Q, Yuan B, Yang S (2023a) Magnetic surface molecularly imprinted polymers for efficient selective recognition and targeted separation of daidzein. Adv Compos Hybrid Mater 6(6):196. https://doi.org/10.1007/s42114-023-00775-5
Wang C, Feng XZ, Shang SB, Liu H, Song ZQ, Zhang HB (2023b) Lignin/sodium alginate hydrogel for efficient removal of methylene blue. Int J Biol Macromol 237:124200. https://doi.org/10.1016/j.ijbiomac.2023.124200
Wang P, Chen X, Gao S, Hu J, Yang L, Song J, Tian H, Lu H, Shi M, Hu X, Chen L, Ding Y, Shi M (2023c) High-performance low-smoke halogen-free flame-retardant composites for Fuxing electric multiple units via synergistic effects of char formation and anti-dripping of clay-based organic sheet silicate. Adv Compos Hybrid Mater 6(3):88. https://doi.org/10.1007/s42114-023-00670-z
Wei JG, Chen YF, Liu HZ, Du CG, Yu HL, Zhou ZX (2016) Thermo-responsive and compression properties of TEMPO-oxidized cellulose nanofiber-modified PNIPAm hydrogels. Carbohyd Polym 147:201–207. https://doi.org/10.1016/j.carbpol.2016.04.015
Wu YJ, Parandoust A, Sheibani R, Kargaran F, Khorsandi Z, Liang YY, Xia CL, Van Le Q (2021) Advances in gum-based hydrogels and their environmental applications. Carbohyd Polym 318:121102. https://doi.org/10.1016/j.carbpol.2023.121102
Xu Q, Wu Z, Zhao W, He M, Guo N, Weng L, Lin Z, Taleb MFA, Ibrahim MM, Singh MV, Ren J, El-Bahy ZM (2023) Strategies in the preparation of conductive polyvinyl alcohol hydrogels for applications in flexible strain sensors, flexible supercapacitors, and triboelectric nanogenerator sensors: an overview. Adv Compos Hybrid Mater 6(6):203. https://doi.org/10.1007/s42114-023-00783-5
Yan JH, Li KR (2021) A magnetically recyclable polyampholyte hydrogel adsorbent functionalized with β-cyclodextrin and graphene

oxide for cationic/anionic dyes and heavy metal ion wastewater remediation. Sep Purif Technol 277:119469. https://doi.org/10.1016/j.seppur.2021.119469

Yang YC, Zhu QL, Peng XW, Sun JJ, Li C, Zhang XM, Zhang H, Chen JB, Zhou XF, Zeng HB, Zhang YL (2022) Hydrogels for the removal of the methylene blue dye from wastewater: a review. Environ Chem Lett 20:2665–2685. https://doi.org/10.1007/s10311-022-01414-z

Yu SS, Lu CM, Tang R, Luo QY, He MY, Zhang HB (2022) Acid activated bentonite-La crosslinked sesbania gum beads for efficient congo red adsorption. International conference on environment, renewable energy and green chemical engineering (EREGCE 2022), vol 350. pp 03009. https://doi.org/10.1051/e3sconf/202235003009

Zhan X-Q, Ran Z-Q, Bao H-Y, Ye Q, Chen H, Fu Q, Ni W, Xu J-M, Ma N, Tsai F-C (2024) Intelligent hydrogel on–off controller sensor for irrigation. Adv Compos Hybrid Mater 7(1):6. https://doi.org/10.1007/s42114-023-00821-2

Zhang F, Lian M, Alhadhrami A, Huang M, Li B, Mersal GAM, Ibrahim MM, Xu M (2022) Laccase immobilized on functionalized cellulose nanofiber/alginate composite hydrogel for efficient bisphenol A degradation from polluted water. Adv Compos Hybrid Mater 5(3):1852–1864. https://doi.org/10.1007/s42114-022-00476-5

Zhu HL, Chen SN, Luo YC (2023a) Adsorption mechanisms of hydrogels for heavy metal and organic dyes removal: a short review. J Agric Food Res 12:100552. https://doi.org/10.1016/j.jafr.2023.100552

Zhu X, Wang Z, Ren J, AlMasoud N, El-Bahy ZM, Alomar TS, Zhang C, Zhang J, Zhou J, Li M, Wang D, Seok I, Guo X (2023b) Graphene/polyacrylamide interpenetrating structure hydrogels for wastewater treatment. Adv Compos Hybrid Mater 6(5):169. https://doi.org/10.1007/s42114-023-00731-3